Quantitative Modeling of the Effect of Oil on Foam for Enhanced Oil Recovery

Tang, Jinyu; Ansari, Mohammed N.; Rossen, William R.

DOI
10.2118/194020-PA

Publication date
2019

Document Version
Final published version

Published in
SPE Journal

Quantitative Modeling of the Effect of Oil on Foam for Enhanced Oil Recovery

Jinyu Tang, Mohammed N. Ansari, and **William R. Rossen,** Delft University of Technology

Summary

The effectiveness of foam for mobility control in the presence of oil is key to foam enhanced oil recovery (EOR). A fundamental property of foam EOR is the existence of two steady-state flow regimes: the high-quality regime and the low-quality regime. Experimental studies have sought to understand the effect of oil on foam through its effect on these two regimes. Here, we explore the effect of oil on the two flow regimes for one widely used foam model.

The STARS (CMG 2015) foam model includes two algorithms for the effect of oil on foam: In the "wet-foam" model, oil changes the mobility of full-strength foam in the low-quality regime, and in the "dry-out" model, oil alters the limiting water saturation around which foam collapses. We examine their effects as represented in each model on the two flow regimes using a Corey relative permeability function for oil. Specifically, we plot the pressure-gradient contours that define the two flow regimes as a function of superficial velocities of water, gas, and oil, and show how oil shifts behavior in the regimes.

The wet-foam model shifts behavior in the low-quality regime with no direct effect on the high-quality regime. The dry-out model shifts behavior in the high-quality regime but not the low-quality regime. At fixed superficial velocities, both models predict multiple steady states at some injection conditions. We perform a stability analysis of these states using a simple 1D simulator with and without incorporating capillary diffusion. The steady state attained after injection depends on the initial state. In some cases, it appears that the steady state at the intermediate pressure gradient is inherently unstable, as represented in the model. In some cases, the introduction of capillary diffusion is required to attain a uniform steady state in the medium. The existence of multiple steady states, with the intermediate one being unstable, is reminiscent of catastrophe theory and of studies of foam generation without oil.

Introduction

Injected gas (carbon dioxide, steam, or hydrocarbon gas) can be very efficient in displacing oil in EOR but suffers from poor sweep efficiency (Lake et al. 2014). Foam is one promising means of increasing the sweep efficiency of injected gas (Schramm 1994; Rossen 1996).

A fundamental property of steady-state foam behavior in porous media, in the absence of oil, is the existence of two steady-state flow regimes: the high- and low-quality regimes **(Fig. 1).** Foam "quality" means gas fractional flow f_g. At high foam quality (upper-left portion of Fig. 1), pressure gradient ∇p is nearly independent of gas superficial velocity U_g. Behavior in this regime is thought to be controlled by foam stability, specifically by foam collapse at a limiting capillary pressure (Khatib et al. 1988; Alvarez et al. 2001). At low foam quality (lower-right portion of Fig. 1), ∇p is nearly independent of liquid superficial velocity U_w. In this regime, foam-bubble size is thought to be fixed at a minimum size close to pore size, and foam mobility is thought to be controlled by capillary trapping and mobilization of bubbles as well as drag on moving bubbles (Hirasaki and Lawson 1985; Falls et al. 1988; Rossen and Wang 1997; Xu and Rossen 2003). The rheology of foam in the two flow regimes of Fig. 1 is usually not consistent (Osterloh and Jante 1992; Cheng et al. 2000; Kim et al. 2005). Foam in the low-quality regime in the absence of oil usually shows shear-thinning behavior with respect to U_g. At fixed f_g, this implies shear-thinning behavior with respect to total superficial velocity U_t. In contrast, the high-quality regime could be either Newtonian, shear thinning, or shear thickening with respect to U_w. One way to examine the rheology in each regime is to measure the pressure gradient by varying total superficial velocity at fixed foam quality. One recent study plotted effective viscosity vs. foam quality at fixed pressure gradients (de Araujo Cavalcante Filho et al. 2018), using information similar to that in Fig. 1. The alignment features of curves on such a plot suggest Newtonian behavior, whereas separate curves reflect either shear-thinning or shear-thickening behavior, depending on the change of effective viscosity with pressure gradient. The rheology of foam can be seen on a contour plot, such as that in Fig. 1. Evenly spaced contours, for the same increase in the pressure gradient, imply Newtonian behavior. Increasingly sparse or dense contours in one of the flow regimes in Fig. 1 suggest either shear-thinning or shear-thickening behavior, respectively, in the given regime. Experimental observations (Tang et al. 2017) suggest that weaker foam with oil in the low-quality regime reflects either a destabilizing effect of oil or shear-thinning behavior, or perhaps both. To avoid confusion, we exclude the factors for representation of non-Newtonian effects in each regime in this modeling study.

An alternative way to plot data and visualize the two flow regimes is in a scan of the apparent viscosity of foam μ_{app} as a function of foam quality f_g, at fixed total superficial velocity U_t **(Fig. 2)** (Ma et al. 2013; Boeije and Rossen 2015). Foam apparent viscosity is defined as the viscosity of foam, treating it as a single phase,

$$\mu_{app} = k|\nabla p|/U_t, \quad (1)$$

where k is permeability. The plot of Fig. 2 is in essence a diagonal slice, cutting through a plot such as Fig. 1 at fixed total superficial velocity $U_t = (U_g + U_w)$. In Fig. 2, the low-quality regime in Fig. 1 corresponds to the left side of the plot, where μ_{app} increases with increasing f_g; the high-quality regime corresponds to the right side, where μ_{app} decreases with increasing f_g. The foam quality at which the transition from the low- to the high-quality regime occurs in Figs. 1 and 2 is defined as transition foam quality f_g^*. For the rest of this paper, we assume that the transition between the two flow regimes is abrupt, giving a relatively sharp corner in the ∇p contours in Fig. 1 and a relatively sharp peak in Fig. 2. This suggests a large value of the adjustable foam parameter *epdry* used in our implicit-texture (IT) foam modeling (see Appendix A for its definition). Given the commercial aspects concerning the stability of numerical simulators and computational cost, some studies assume a small value of *epdry* (Ma et al. 2013; Farajzadeh et al. 2015; Zeng et al. 2016; Al Sumaiti et al. 2017), which sometimes does not give an ideal match to data.

Original SPE manuscript received for review 11 December 2017. Revised manuscript received for review 16 July 2018. Paper (SPE 194020) peer approved 31 July 2018.

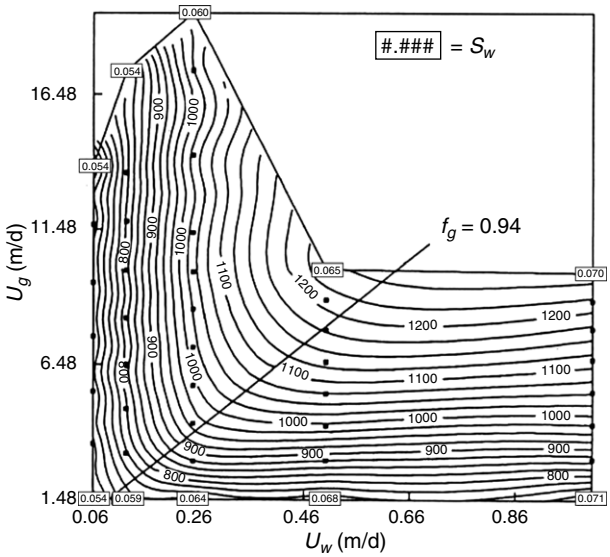

Fig. 1—Pressure drop across a 2-ft sandpack as a function of superficial velocities of gas (U_g) and water (U_w). The pressure gradient in psi/ft is one-half the values shown. Contours of equal pressure drop are plotted through steady-state data, which are represented by black points. This figure is adapted from Osterloh and Jante (1992).

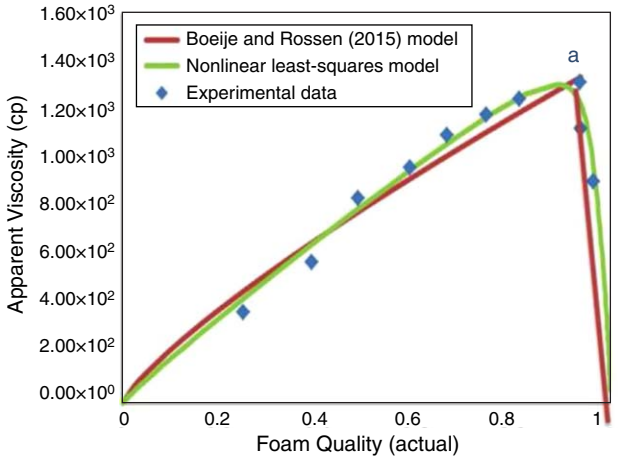

Fig. 2—Apparent viscosity of foam without oil at fixed total superficial velocity (0.671 ft/D) in a 90-md Berea core, as a function of foam quality, from Kapetas et al. (2017). The green least-squares model fit finds an abrupt, although continuous, transition between the two flow regimes; the red fit assumes an infinitely abrupt transition.

Because of the lack of data and complexity of interactions between foam and oil, the effect of oil on foam stability is not yet fully understood (Farajzadeh et al. 2012). Initial efforts to understand the effect of oil on foam represent surface phenomena and phase behavior using entering, spreading, and bridging coefficients as well as the "lamellae number" (Harkins and Feldman 1922; Garrett 1979; Frye and Berg 1989; Bergeron et al. 1993; Dalland et al. 1994; Kruglyakov and Vilkova 1999). However, none of these factors individually or in a combination yet discovered is a good criterion to quantitatively predict the effect of oil on foam (Basheva et al. 2000). One way to study the effect of oil on foam is to conduct dynamic coreflood displacements with an initial oil saturation in the core. Most of the previous experimental studies focused either on foam displacements with oil (Hahn et al. 1985; Simjoo and Zitha 2013) or on steady-state foam flow in the presence of residual oil (Myers and Radke 2000). Foam strength in these studies was mostly evaluated in terms of pressure-gradient responses with oil saturation either varying in a transient displacement or fixed at residual. However, none of these studies could effectively quantify the effect of oil on foam over a range of oil saturations or fractional flows. Interpreting these experiments in terms of the effect of oil saturation on foam is complicated by the change in oil saturation in the core during the displacement. This raises some key issues in simulating foam EOR processes, such as how to properly describe the effect of oil on foam in models, as well as whether current models suitably represent the effect of oil on foam. Without answering these questions, the selection of a suitable foam model for foam EOR and the estimation of oil parameters in foam models cannot be achieved properly and efficiently. Because the two flow regimes identified for local equilibrium (LE) foam flow in the absence of oil are already well-understood, experiments have sought to understand the effect of oil on foam through its effect on the two foam-flow regimes. In the experiments of Rong (2002) and of Shen et al. (2006), oil superficial velocity was maintained as a fixed fraction of water superficial velocity. Another possibility would be to maintain oil superficial velocity as fixed, regardless of superficial velocities of water and gas. A third possibility is to represent the two flow regimes at fixed oil saturation. In general, however, oil saturation is not known or controlled in a coreflood experiment. The step after collecting experimental data is to fit a foam model to data and evaluate the suitability of current foam models for representing the effect of oil on foam.

To interpret such data in terms of models, it is necessary first to understand how those models represent the effect of oil on foam when plotted in a manner similar to Fig. 1 or Fig. 2. Among the two groups of foam models (IT and population-balance foam models),

only the IT foam models in the STARS simulator describe the effect of oil on foam explicitly. A previous study (Myers and Radke 2000) incorporated the effect of oil on foam in a population-balance model by reducing bubble-generation rate, accounting for a reduction in generation sites caused by oil occupancy. This does not reflect the effect of oil saturation and composition on the stability of foam with oil. Comparisons of the IT and population-balance approaches to foam modeling can be found in Ma et al. (2015) and Lotfollahi et al. (2016a). One major goal of this study is to show how the widely used foam model in the STARS simulator represents foam behavior in the presence of oil. Other IT foam models have similar algorithms. The STARS model assumes instantaneous attainment of LE between rates of creation and destruction of foam. Specifically, in modeling the effect of oil on foam through its effect on the two flow regimes in Fig. 1, we consider the three approaches proposed previously to measure the effect of oil: fixed oil saturation, fixed oil superficial velocity, and fixed oil/water-superficial-velocity ratio. Here, we mainly illustrate how oil shifts the two flow regimes with changing values of the relevant parameters, rather than a sensitivity analysis of parameters. The theoretical analyses given in this paper are mostly consistent with our experimental observations in a companion study (Tang et al. 2017). In some cases, we identify multiple steady states predicted by the model for the same injection conditions. A simple 1D incompressible simulator is then developed to analyze the stability of the multiple steady states. A third steady state is revealed by the simulation results.

Lastly, we present the multiple steady states as a surface of effective viscosity as a function of fractional flows and saturations, respectively, on a ternary diagram. The folding of this surface is reminiscent of catastrophe theory (Zeeman 1977) and is similar to the multiple steady states seen as a function of pressure gradient in studies of foam generation without oil (Gauglitz et al. 2002; Kam and Rossen 2003; Lotfollahi et al. 2016b). The multiple steady states predicted in the foam models need further study to verify their existence experimentally and to test their stability.

Results and Analysis

Gas mobility, the ratio of gas permeability to gas viscosity, is reduced by foam. In simulation, this mobility reduction can be represented either by reducing gas relative permeability or by increasing gas viscosity. In the STARS foam model (see Appendix A), gas-mobility reduction by foam is represented as a reduction in gas relative permeability. The effective gas relative permeability with foam is the product of the foam-free gas relative permeability and a mobility factor (FM). FM in turn is inversely proportional to the product of a series of functions accounting for the effects of surfactant concentration, non-Newtonian foam mobility, water saturation (and, by implication, capillary pressure), and oil saturation. In this paper, for simplicity we neglect all effects except the effects of water saturation (dry-out) and oil saturation. The equations given in the STARS foam model account for the effect of oil on foam in two ways. In the wet-foam model, the mobility reduction of full-strength foam is reduced with increasing oil saturation. In the dry-out model, increasing oil saturation causes the water saturation at which foam collapses to increase (by implication, reflecting a decrease in the limiting capillary pressure, and therefore less-stable foam). Details are given in Appendix A. The definitions of all foam parameters involved in this study and the values used are provided in Appendix A. Note that different names are used for similar parameters in the two models. For instance, the limiting water saturation in the wet-foam model is *fmdry,* and in the dry-out model is *sfdry*. The oil parameters *fmoil, floil,* and *epoil* in the wet-foam model are expressed as *sfoil, sloil,* and *efoil* in the dry-out model.

The Oil Effect Represented in the STARS Foam Model. ***Oil Effect Predicted by Wet-Foam Model.*** **Fig. 3** illustrates how the wet-foam model reflects foam performance at fixed oil saturation when the oil-related parameters *fmoil, floil,* and *epoil* vary. The LE foam-flow behavior implied by the wet-foam model continues to show the two flow regimes in the presence of oil. The nearly horizontal pressure-gradient contours in the low-quality regime shift upward or downward as the parameters in the wet-foam model vary. In contrast, the pressure-gradient contours in the high-quality regime remain unchanged as the model parameters change.

Fig. 4 illustrates similar behavior for a fixed oil superficial velocity (5 ft/D). The contours in the low-quality regime shift up or down in response to model parameters, with little or no effect on the high-quality regime. In contrast to Fig. 3, oil saturation is not fixed in these plots, but depends on pressure gradient. With oil superficial velocity fixed and using a Corey expression for oil relative permeability, the oil saturation is fixed along a given pressure-gradient contour, but decreases with increasing pressure gradient. The effect of increasing oil saturation with decreasing ∇p is seen indirectly in the shift of the ∇p contours in the plots.

Fig. 5 illustrates behavior when oil is injected at a fixed oil/water-superficial-velocity ratio. In this case, oil saturation increases along a ∇p contour as water superficial velocity increases in the low-quality regime. Thus, as illustrated in Fig. 5b, ∇p contours can bend upward in the low-quality regime, reflecting greater mobility of full-strength foam as oil saturation increases. Vertical contours in the high-quality regime are at nearly fixed water superficial velocity, and therefore oil superficial velocity and oil saturation are fixed also. As a result, the parameters in the wet-foam model again alter only the low-quality regime.

Oil Effect Predicted by Dry-Out Model. **Fig. 6** illustrates foam-flow behavior reflected by the dry-out model at fixed oil saturation, corresponding to different sets of oil model parameters. As with the wet-foam model, the two flow regimes continue to appear as parameters change. However, in contrast to the wet-foam model, the parameters in the dry-out model affect only the high-quality regime. This is true also for plots at fixed oil superficial velocity **(Fig. 7)** and fixed oil/water-superficial-velocity ratio **(Fig. 8).**

Foam-Quality Scan With Varying U_o/U_w Ratios. In plots of ∇p as a function of gas and water superficial velocities, if the boundary between foam regimes is sharp, then adjusting the parameters of the wet-foam model shifts the low-quality regime, and changing parameters in the dry-out model alters the high-quality regime. As noted, another popular way to represent the two regimes is in a scan of gas superficial velocity at fixed total superficial velocity (Fig. 2). In at least one case, such a scan can be misleading when oil is included. **Fig. 9** shows a plot of foam apparent viscosity as a function of foam quality f_g with varying oil/water-superficial-velocity ratios. In this case, "foam quality" means gas superficial velocity as a fraction of total superficial velocity including oil {i.e., $[U_g/(U_g+U_w+U_o)]$}. Only the wet-foam model is implemented here, with the parameter values indicated. For these parameters, the effect of oil on the low-quality regime is modest. It appears that oil has a strong effect on the high-quality regime, but this is misleading. The water saturation at which foam collapses is independent of the oil/water-superficial-velocity ratio (U_o/U_w) in this case. As this ratio increases, however, the superficial velocity of water at a given value of f_g decreases, because $f_g = U_g/(U_g+U_w+U_o)$. It is this decrease in water superficial velocity as U_o/U_w increases, not a collapse of foam, which causes the shift in this plot with U_o/U_w. In other words, U_o/U_w has no direct effect on the high-quality regime.

Multiple Steady States. ***Wet-Foam Model.*** **Fig. 10** shows the behavior in the wet-foam model with oil superficial velocity fixed for one set of oil-related-parameter values. As seen previously, the pressure-gradient contours in the high-quality regime are independent of the oil-related parameters in the wet-foam model. However, contours with a lower pressure gradient in the low-quality regime (e.g., the contour of 200 psi/ft in Fig. 10) shift upward, crossing contours with a higher pressure gradient in the high-quality regime. There are multiple steady states for the injection condition at the point of intersection.

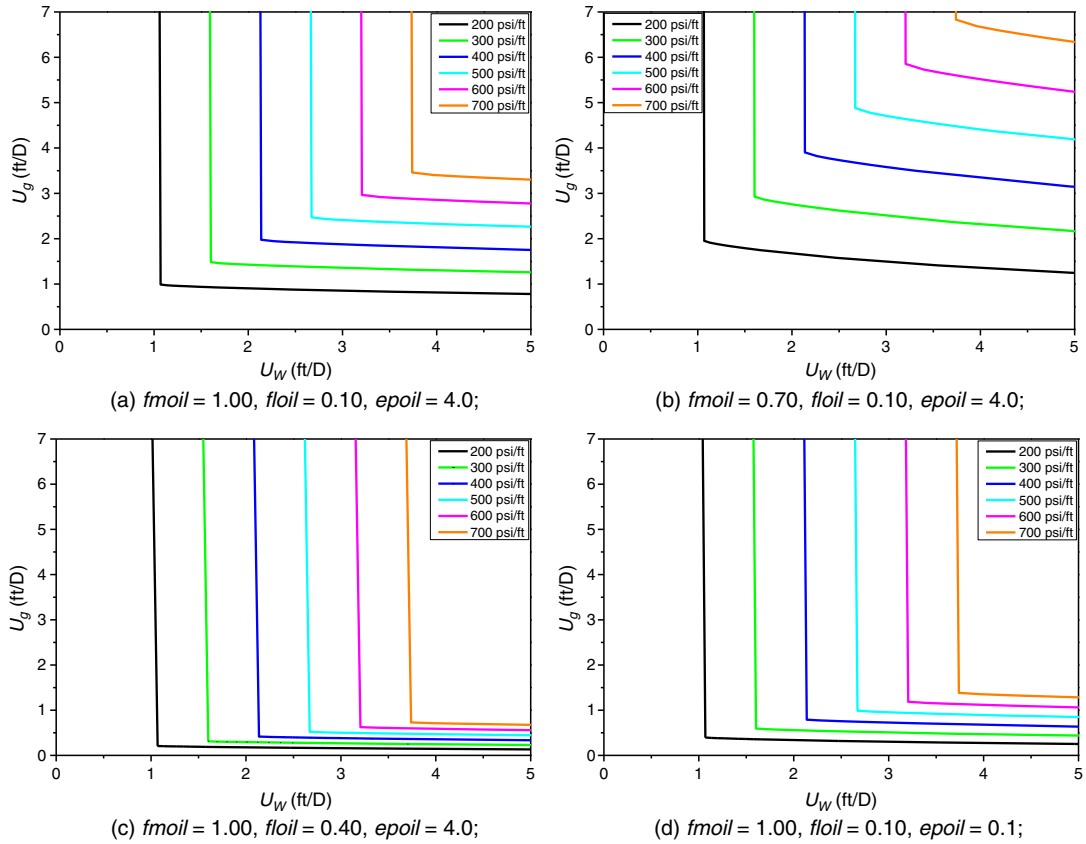

(a) *fmoil* = 1.00, *floil* = 0.10, *epoil* = 4.0; (b) *fmoil* = 0.70, *floil* = 0.10, *epoil* = 4.0;

(c) *fmoil* = 1.00, *floil* = 0.40, *epoil* = 4.0; (d) *fmoil* = 1.00, *floil* = 0.10, *epoil* = 0.1;

Fig. 3—Pressure gradient as a function of water and gas superficial velocities predicted by the wet-foam model at fixed oil saturation $S_o = 0.3$, with different values for oil parameters. (a) *fmoil* = 1.00, *floil* = 0.10, *epoil* = 4.0; (b) *fmoil* = 0.70, *floil* = 0.10, *epoil* = 4.0; (c) *fmoil* = 1.00, *floil* = 0.40, *epoil* = 4.0; (d) *fmoil* = 1.00, *floil* = 0.10, *epoil* = 0.1.

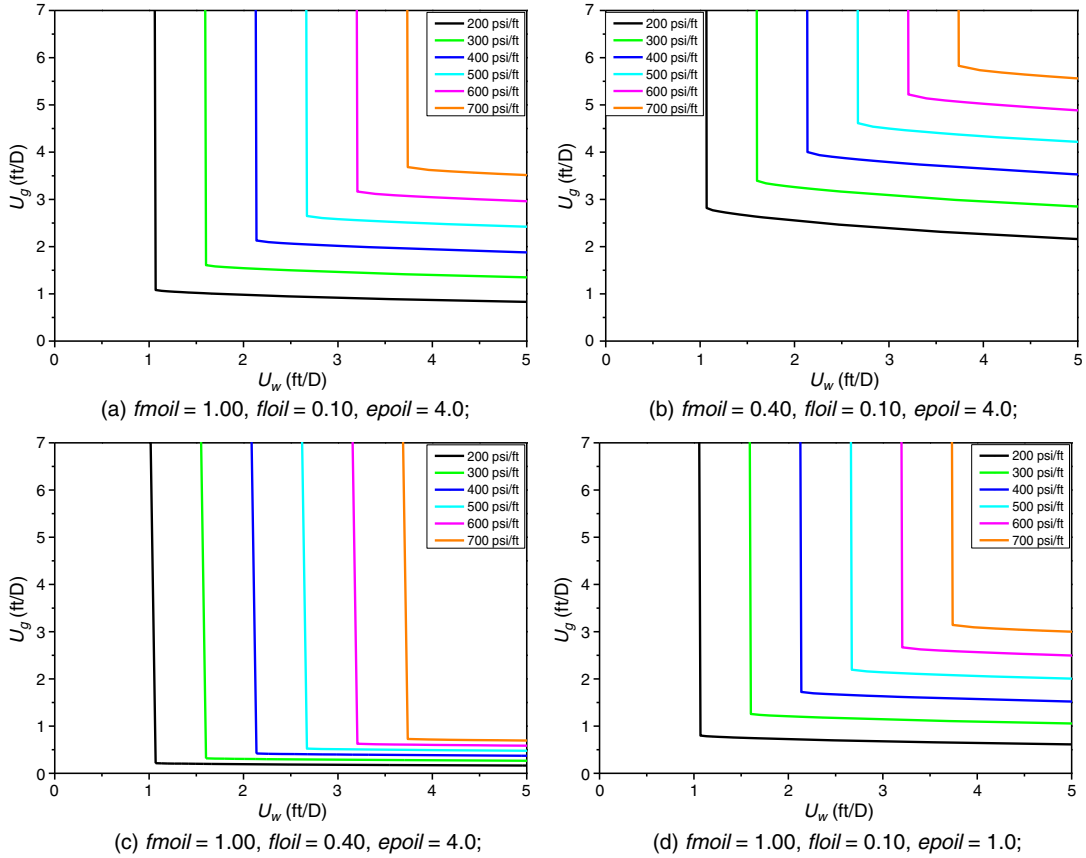

(a) *fmoil* = 1.00, *floil* = 0.10, *epoil* = 4.0; (b) *fmoil* = 0.40, *floil* = 0.10, *epoil* = 4.0;

(c) *fmoil* = 1.00, *floil* = 0.40, *epoil* = 4.0; (d) *fmoil* = 1.00, *floil* = 0.10, *epoil* = 1.0;

Fig. 4—Pressure gradient as a function of water and gas superficial velocities predicted by the wet-foam model at fixed oil superficial velocity $U_o = 5$ ft/D, with different sets of oil-related parameters. (a) *fmoil* = 1.00, *floil* = 0.10, *epoil* = 4.0; (b) *fmoil* = 0.40, *floil* = 0.10, *epoil* = 4.0; (c) *fmoil* = 1.00, *floil* = 0.40, *epoil* = 4.0; (d) *fmoil* = 1.00, *floil* = 0.10, *epoil* = 1.0.

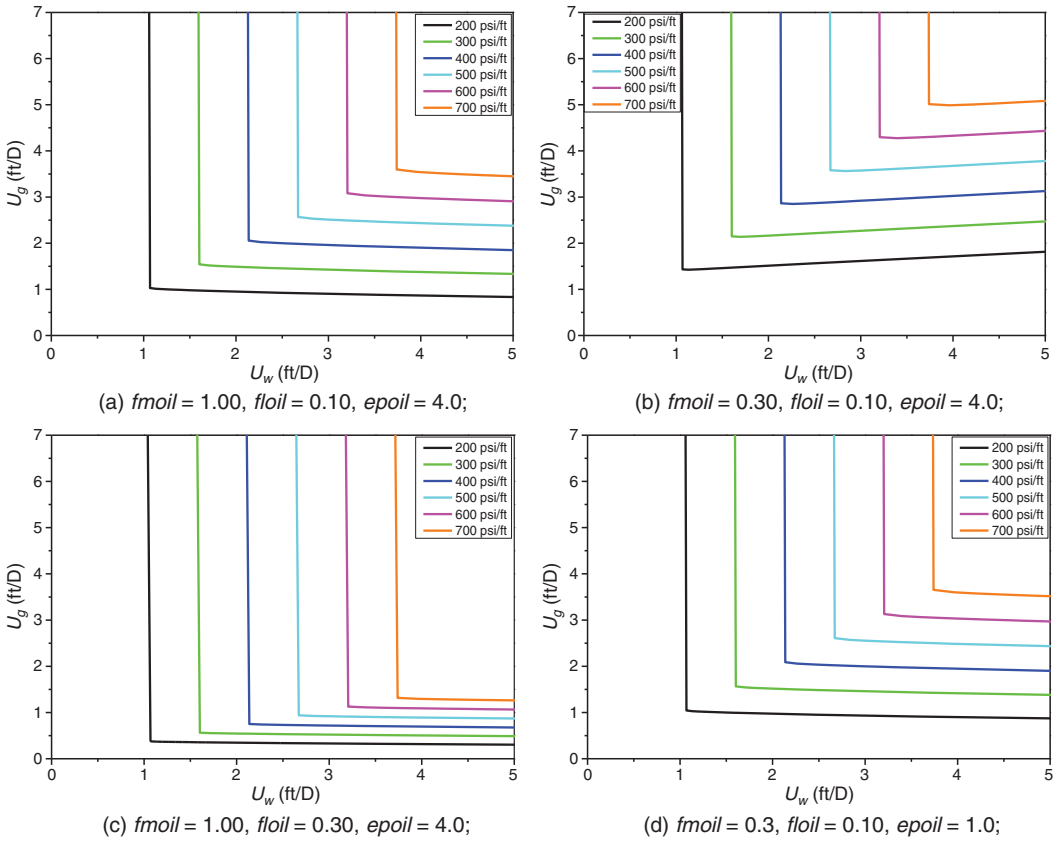

Fig. 5—Pressure gradient as a function of water and gas superficial velocities predicted by the wet-foam model at fixed oil/water-superficial-velocity ratio $U_o/U_w = 0.25$, with changing oil-related parameters. (a) *fmoil* = 1.00, *floil* = 0.10, *epoil* = 4.0; (b) *fmoil* = 0.30, *floil* = 0.10, *epoil* = 4.0; (c) *fmoil* = 1.00, *floil* = 0.30, *epoil* = 4.0; (d) *fmoil* = 0.3, *floil* = 0.10, *epoil* = 1.0.

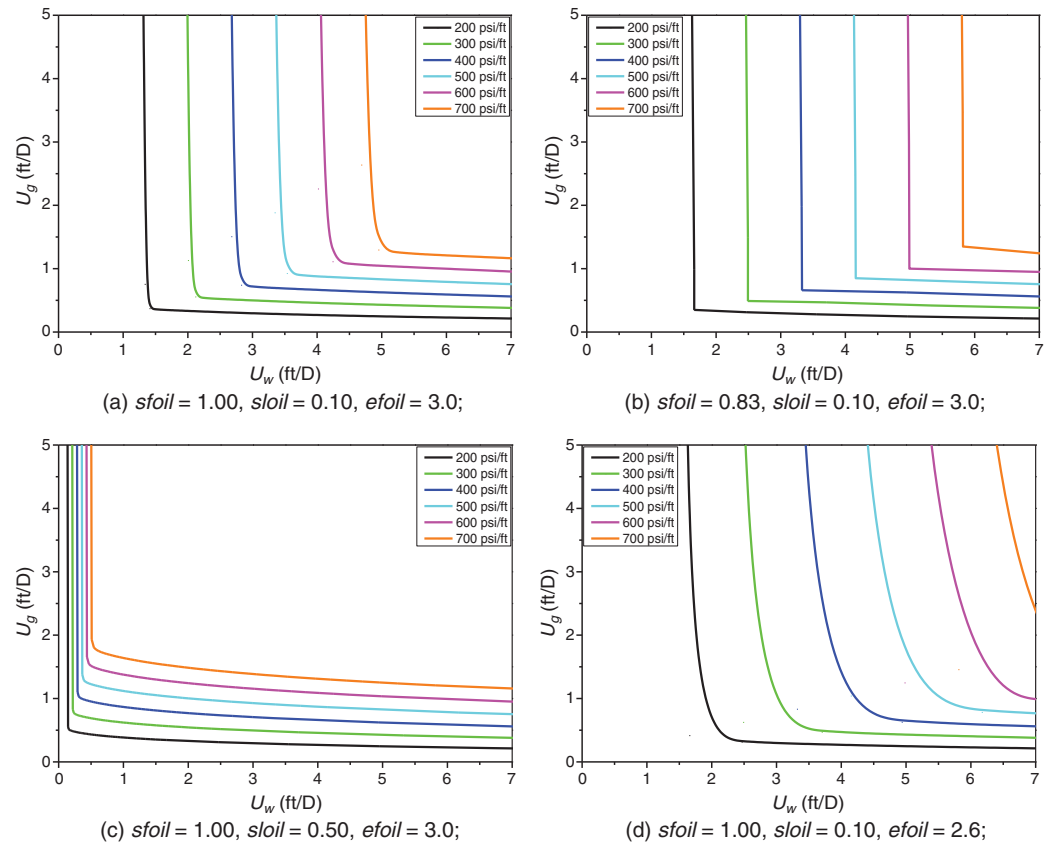

Fig. 6—Pressure gradient as a function of water and gas superficial velocities predicted by the dry-out model at fixed oil saturation $S_o = 0.3$, with different values of oil-related parameters. (a) *sfoil* = 1.00, *sloil* = 0.10, *efoil* = 3.0; (b) *sfoil* = 0.83, *sloil* = 0.10, *efoil* = 3.0; (c) *sfoil* = 1.00, *sloil* = 0.50, *efoil* = 3.0; (d) *sfoil* = 1.00, *sloil* = 0.10, *efoil* = 2.6.

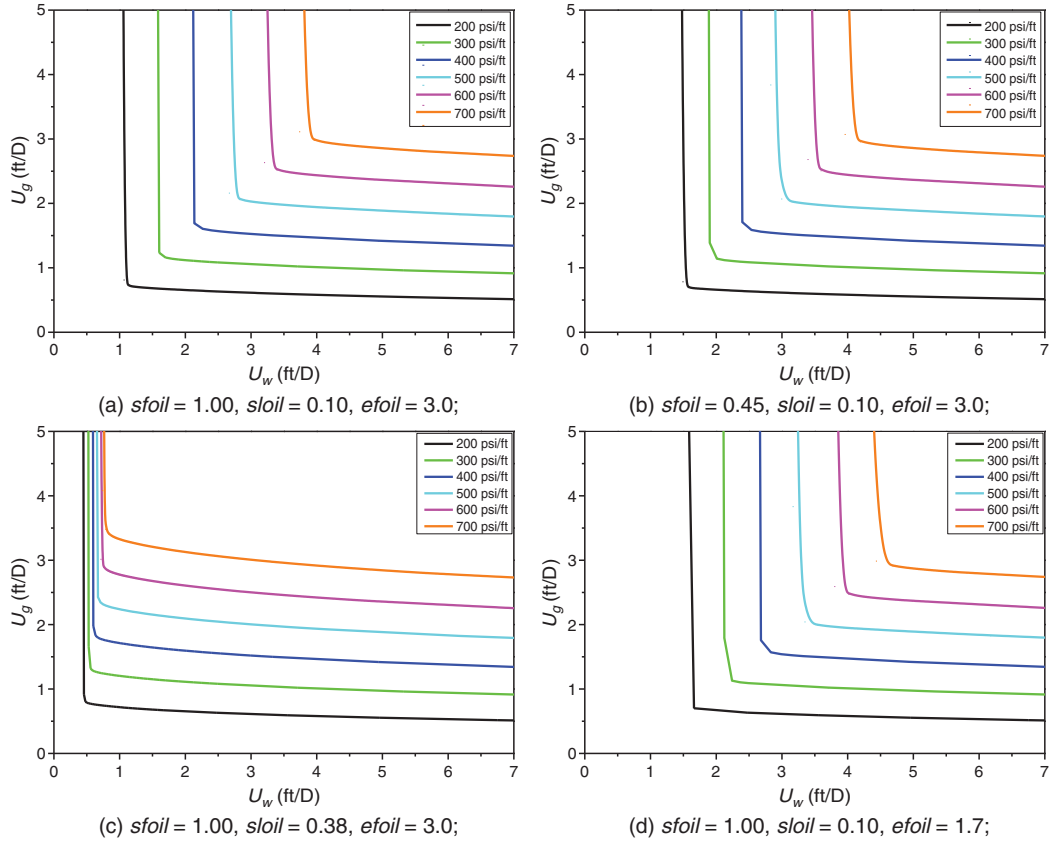

(a) *sfoil* = 1.00, *sloil* = 0.10, *efoil* = 3.0; (b) *sfoil* = 0.45, *sloil* = 0.10, *efoil* = 3.0;

(c) *sfoil* = 1.00, *sloil* = 0.38, *efoil* = 3.0; (d) *sfoil* = 1.00, *sloil* = 0.10, *efoil* = 1.7;

Fig. 7—Pressure gradient as a function of water and gas superficial velocities predicted by the dry-out model at fixed oil superficial velocity $U_o = 5$ ft/D, with different sets of oil-related parameters. (a) *sfoil* = 1.00, *sloil* = 0.10, *efoil* = 3.0; (b) *sfoil* = 0.45, *sloil* = 0.10, *efoil* = 3.0; (c) *sfoil* = 1.00, *sloil* = 0.38, *efoil* = 3.0; (d) *sfoil* = 1.00, *sloil* = 0.10, *efoil* = 1.7.

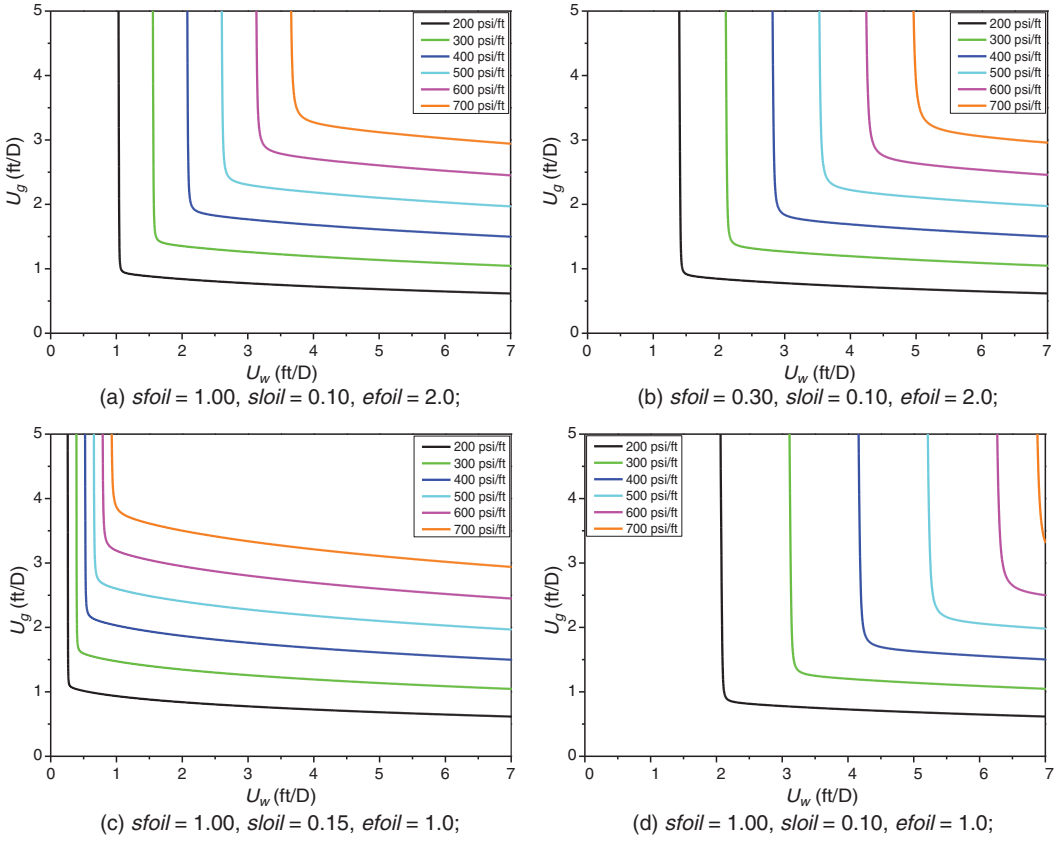

(a) *sfoil* = 1.00, *sloil* = 0.10, *efoil* = 2.0; (b) *sfoil* = 0.30, *sloil* = 0.10, *efoil* = 2.0;

(c) *sfoil* = 1.00, *sloil* = 0.15, *efoil* = 1.0; (d) *sfoil* = 1.00, *sloil* = 0.10, *efoil* = 1.0;

Fig. 8—Pressure gradient as a function of water and gas superficial velocities predicted by the dry-out model at fixed oil/water-superficial-velocity ratio, $U_o/U_w = 0.25$, with different sets of oil-related parameters. (a) *sfoil* = 1.00, *sloil* = 0.10, *efoil* = 2.0; (b) *sfoil* = 0.30, *sloil* = 0.10, *efoil* = 2.0; (c) *sfoil* = 1.00, *sloil* = 0.15, *efoil* = 1.0; (d) *sfoil* = 1.00, *sloil* = 0.10, *efoil* = 1.0.

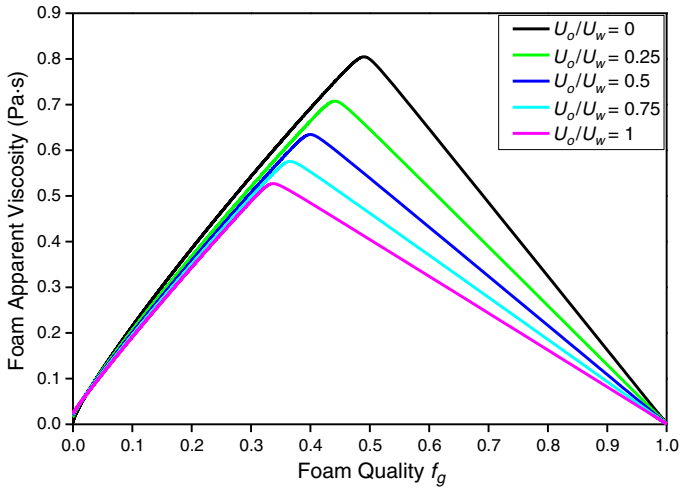

Fig. 9—Foam apparent viscosity vs. foam quality with varying oil/water-superficial-velocity ratios with the wet-foam model. Parameter values are *fmoil* = 1, *floil* = 0.1, *epoil* = 4, and U_t = 13.56 ft/D.

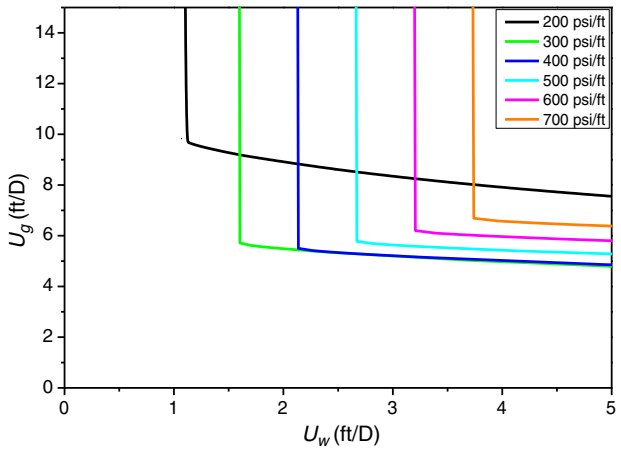

Fig. 10—Multiple steady states predicted by the wet-foam model; pressure-gradient contours plotted as a function of gas and water superficial velocities with fixed oil superficial velocity (5 ft/D). Parameter values are *fmoil* = 0.2, *floil* = 0.1, *epoil* = 1.3.

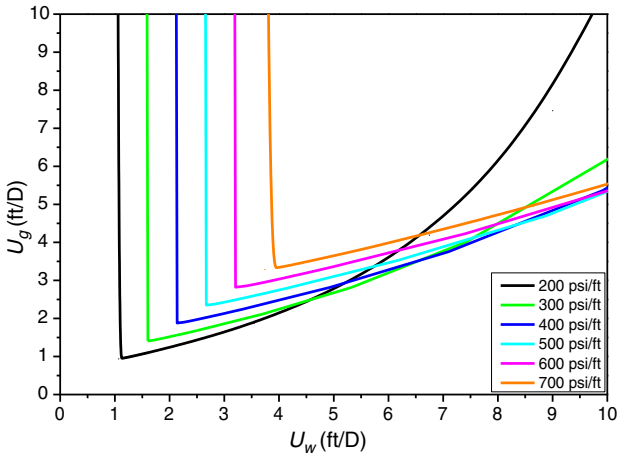

Fig. 11—Multiple steady states predicted by the wet-foam model; pressure-gradient contours plotted as a function of gas and water superficial velocities with fixed oil/water-superficial-velocity ratio (0.25). Parameter values are *fmoil* = 0.2, *floil* = 0.12, *epoil* = 4.

According to Darcy's law, with a Corey function for oil relative permeability, oil superficial velocity is a function of oil saturation and pressure gradient. At fixed oil superficial velocity, decreasing pressure gradient means increasing oil saturation. In other words, the effect of oil on foam in the low-quality regime is greater along the lower-pressure-gradient contour. This contour in the low-quality regime moves upward, intersecting other pressure-gradient contours, thereby yielding multiple steady states.

Fig. 11 shows the pressure-gradient contours for a case with a fixed oil/water-superficial-velocity ratio. Here, the pressure-gradient contours in the low-quality regime tilt upward at higher water superficial velocity, crossing other pressure-gradient contours. Along

each pressure-gradient contour in the low-quality regime, with a fixed oil/water-superficial-velocity ratio, oil saturation increases with increasing water superficial velocity, implying a greater effect on foam mobility. Oil saturation falls with increasing pressure gradient for a given water superficial velocity, with less effect on foam. This leads to multiple states for some injection conditions.

Dry-Out Model. **Fig. 12** shows multiple steady states using the dry-out model with oil superficial velocity fixed. In the dry-out model, oil affects only the high-quality regime. Increasing water superficial velocity along a $\bigtriangledown p$ contour first leads the contours to a change from the high-quality regime to the low-quality regime. However, some contours with a lower pressure gradient (e.g., contours of 200, 300, or 400 psi/ft) shift from the high-quality to the low-quality regime at higher water superficial velocity than some other contours with a higher pressure gradient (500, 600, or 700 psi/ft), resulting in intersections between the contours—and hence multiple steady states.

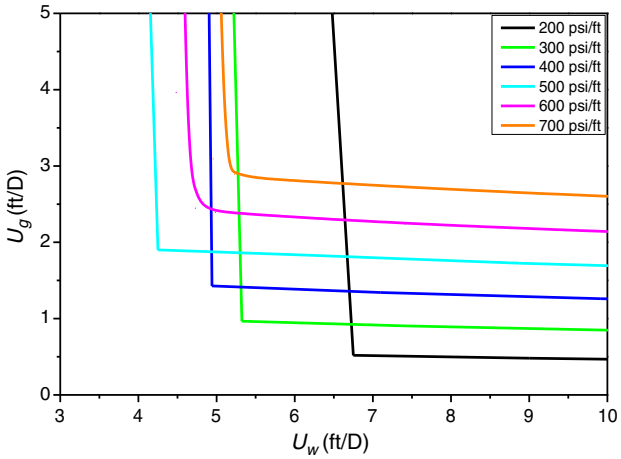

Fig. 12—Multiple steady states predicted by the dry-out model; pressure-gradient contours plotted as a function of gas and water superficial velocities with fixed oil superficial velocity (5 ft/D). Parameter values are *sfoil* = 0.3, *sloil* = 0.1, *efoil* = 3.

The limiting water saturation in the dry-out model is not constant, but increases with increasing oil saturation. This increase in oil saturation destabilizes foam, causing pressure-gradient contours in the high-quality regime to shift to the right. With oil superficial velocity fixed in the dry-out model, oil saturation increases with decreasing pressure gradient; a lower pressure gradient thus yields a greater limiting water saturation and a weaker foam. If this effect is strong enough, a vertical contour in the high-quality regime can shift to a larger water superficial velocity with decreasing $\bigtriangledown p$. This can cause multiple steady states.

With a fixed oil/water-superficial-velocity ratio, oil saturation rises with increasing water superficial velocity along a $\bigtriangledown p$ contour **(Fig. 13).** As a result, both oil and water saturations increase with increasing U_w in the low-quality regime. The increase in oil saturation causes an increase in limiting water saturation in the dry-out model. If the limiting water saturation increases enough, foam re-enters the high-quality regime again at higher U_w. The contours with a lower pressure gradient re-enter the high-quality regime at a relatively lower water superficial velocity than the contours at a higher pressure gradient, causing intersections of contours and multiple steady states. This shift of water saturation and limiting water saturation along the low-quality regime is illustrated in **Figs. 14 and 15.**

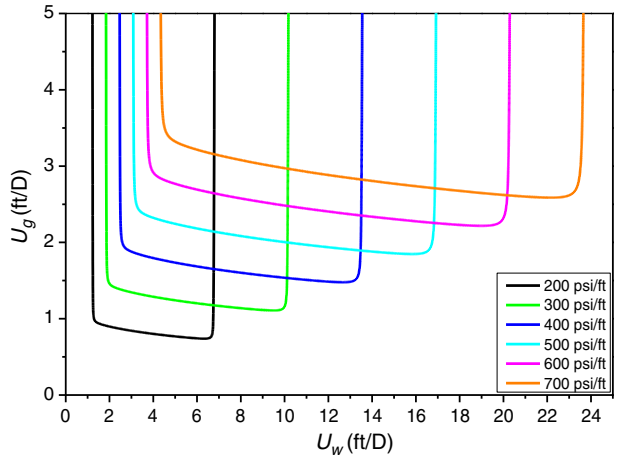

Fig. 13—Multiple steady states predicted by the dry-out model; pressure-gradient contours plotted as a function of gas and water superficial velocities with fixed oil/water-superficial-velocity ratio (0.04). Parameter values are *sfoil* = 0.144, *sloil* = 0.1, *efoil* = 3.

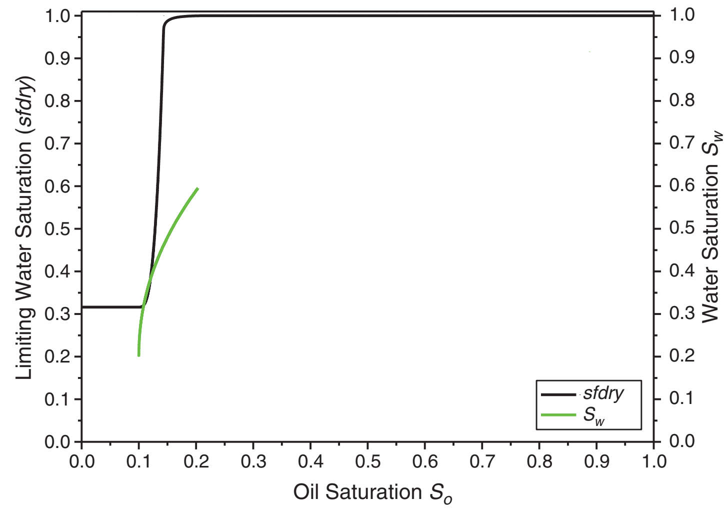

Fig. 14—Comparison between limiting water saturation *sfdry* (see Appendix A) and water saturation S_w as oil saturation changes in Fig. 13. The first high-quality regime is at the leftward intersection point, and the second at the rightward intersection point. The low-quality regime in Fig. 13 is the interval between these two intersection points. Parameter values are *sfoil* = 0.144, *sloil* = 0.1, *efoil* = 3, and U_o/U_w = 0.04.

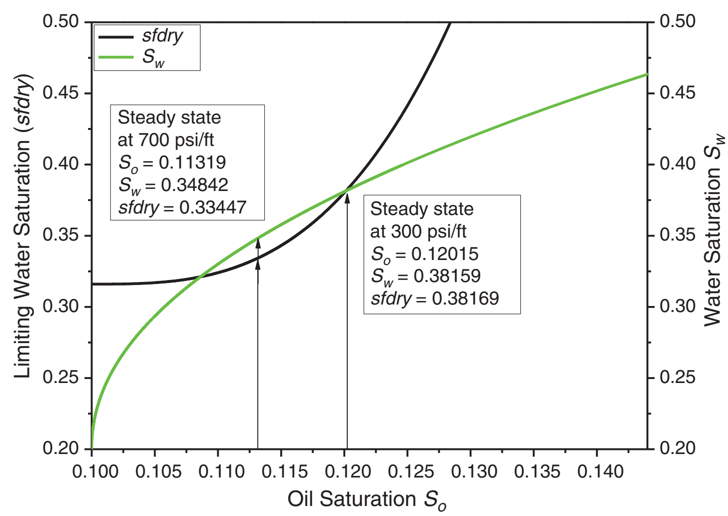

Fig. 15—Enlarged view of Fig. 14, around the intersection points and the interval between them.

Simulation Analysis of Multiple Steady States. ***Stability Analysis.*** Both the wet-foam and dry-out models, with a fixed oil superficial velocity and a fixed oil/water-superficial-velocity ratio, predict multiple steady states for some injection conditions in the presence of oil. Each set of multiple steady states corresponds to different foam strength, but has the same fractional flows.

We next address the stability of the steady states at the intersection of pressure-gradient contours of 300 and 700 psi/ft for the dry-out model with a fixed oil/water-superficial-velocity ratio, shown previously in Fig. 13 and again in **Fig. 16.** We examine first which steady state is obtained for the given initial conditions, and then the stability of the two states to perturbations in 1D flow.

A simple 1D simulator (100×1×1 gridblocks) was developed with the following assumptions: homogeneous reservoir, incompressible fluids and matrix, isothermal process, negligible effect of gravity, upstream weighting, and initially excluding capillary diffusion. It is further assumed that surfactant is present throughout the water phase, and foam immediately takes its LE properties. The governing set of equations is then of the form

$$S_{p,i}^{t+\Delta t} = S_{p,i}^{t} + \frac{\Delta t \times U_t}{\phi \times \Delta x}\left(f_{p,i-1}^{t} - f_{p,i}^{t}\right) \quad (2)$$

where the subscript p denotes phase, the subscript i is the gridblock (of length Δx), Δt is timestep, ϕ is porosity, and f_p is fractional flow for each phase in the given gridblock at the given time. Both the wet-foam and dry-out models were examined, and yield consistent results regarding the stability of the multiple steady states. Here, we present the stability analysis using the dry-out model. For our study, the dry-out foam model described in Appendix A is incorporated into the fractional-flow expression of each phase in the simple 1D simulator. Gas mobility is modified by foam using the mobility-reduction factor *fmmob* and limiting water saturation *sfdry,* where water- and oil-saturation-dependent functions are considered in the simulation. All the parameters used in the numerical stability analysis are given in Appendix A. Specifically, the set of fractional flows into the first gridblock, f_{p0}, was set at the injection condition for the steady states. For the stability analysis, the initial saturation is uniform at one of the steady states, with a small random perturbation in saturations (less than 0.01) added to 10 randomly selected gridblocks. We also tested what steady state the system reaches for three

uniform initial states (each at residual saturation for all but one of the phases). **Table 1** specifies the injection and initial conditions for each case. Our interpolation for the superficial velocities at the intersection point in Fig. 16 was inexact, so in fact the two steady states with the given superficial velocities have pressure gradients of 300 and approximately 706 psi/ft in the simulations.

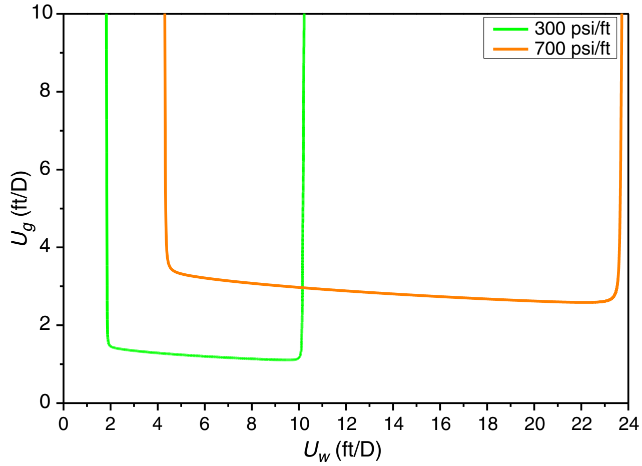

Fig. 16—Intersection of contours of 300 and 700 psi/ft, from Fig. 13.

Scenario No.		Injection Condition (ft/D)			Initial States		
		U_w	U_o	U_g	S_w	S_o	S_g
1	$S_{w,max}$	10.15110	0.40604	2.99894	0.7	0.1	0.2
2	$S_{o,max}$				0.2	0.6	0.2
3	$S_{g,max}$				0.2	0.1	0.7
4	300 psi/ft				0.38159	0.12015	0.49826
5	700 psi/ft				0.34842	0.11319	0.53839

Table 1—Overview of five simulation scenarios involving the two states at the intersection of 300- and 700-psi/ft contours from Fig. 13.

Fig. 17 shows the final states obtained after injecting 10 pore volumes (PVs) corresponding to the five scenarios listed in Appendix A, using the 1D simulator without capillary diffusion. During the process of three-phase flooding, some oscillations appear along the reservoir moving downstream before reaching a steady state. By comparing all the ultimate saturation profiles achieved with the injection condition tested, the five scenarios starting with different initial states end up with two final states in terms of saturations: one final state close to the steady state of 700 psi/ft and a new steady state unidentified previously. The steady state at 300 psi/ft is not present at the end in any case, even when it is the initial state. The steady state at 300 psi/ft is evidently unstable to perturbations; the stability of the state at 706 psi/ft is not clear.

The final states in the two stability tests (Figs. 17d and 17e) are not uniform. There is a jump from the state at 706 psi/ft to one at 11.33 psi/ft some distance down from the inlet, which appears to remain fixed in place over time. In the absence of diffusion or dispersion, with multiple steady states sharing the same fractional flows, it is possible that two consecutive gridblocks at different saturation could have the same fractional flows and thus not change with time. Nothing in our simulation model reflects a particular length scale, however. Thus, these fluctuations could occur over lengths of millimeters or less, in which case capillary diffusion would be dominant.

Therefore, we modified the simulator to allow in a qualitative manner for diffusion (which could arise from gradients in capillary pressure). For simplicity, we use constant diffusion coefficients, giving the following expressions for fractional flows,

$$f_{w,D}(i) = f_w(i) - D_w\left[\frac{S_w(i+1) - S_w(i)}{\Delta x}\right],$$

$$f_{g,D}(i) = f_g(i) - D_g\left[\frac{S_g(i+1) - S_g(i)}{\Delta x}\right],$$

$$f_{o,D}(i) = 1 - f_{w,D}(i) - f_{g,D}(i), \quad \text{(3)}$$

where the subscript D indicates fractional flow accounting for diffusion and D_w and D_g are the diffusion coefficients for water and gas, respectively. The displacements in **Figs. 18a through 18c** at 0.1 PV show that the diffusion coefficients are sufficient to disperse the front over several gridblocks but leave it otherwise intact. Displacements starting with high oil or water saturation end with the newly identified state, whereas one starting with maximum gas saturation ends at the 706-psi/ft state. The jumps in the final case in the stability tests, Figs. 17d and 17e, disappear with the following results: the 300-psi/ft steady state is unstable and the 706-psi/ft state is stable. The newly identified steady state is at water saturation $S_w = 0.5951$. It shows a pressure gradient of only 11.33 psi/ft; oil saturation is greater than that at which foam is completely destroyed. We find this same steady state with the foam model disabled. To confirm that the form of the perturbations did not control stability, we conducted additional simulations with sinusoidal perturbations of maximum magnitude of 0.005 in saturation that have wavelength at either twice or one-half the system length. The final results were the same as in Figs. 18d and 18e. An additional simulation with the newly identified steady state as the initial state confirms that it is stable to small

perturbations. Simulation-stability analysis for another instance (i.e., the intersection of the 300- and 600-psi/ft contours), achieves similar results, as shown in **Table 2.** Again, three steady states exist for the same injection condition, with upper and lower steady states being stable to perturbation in saturations but the intermediate steady state being unstable.

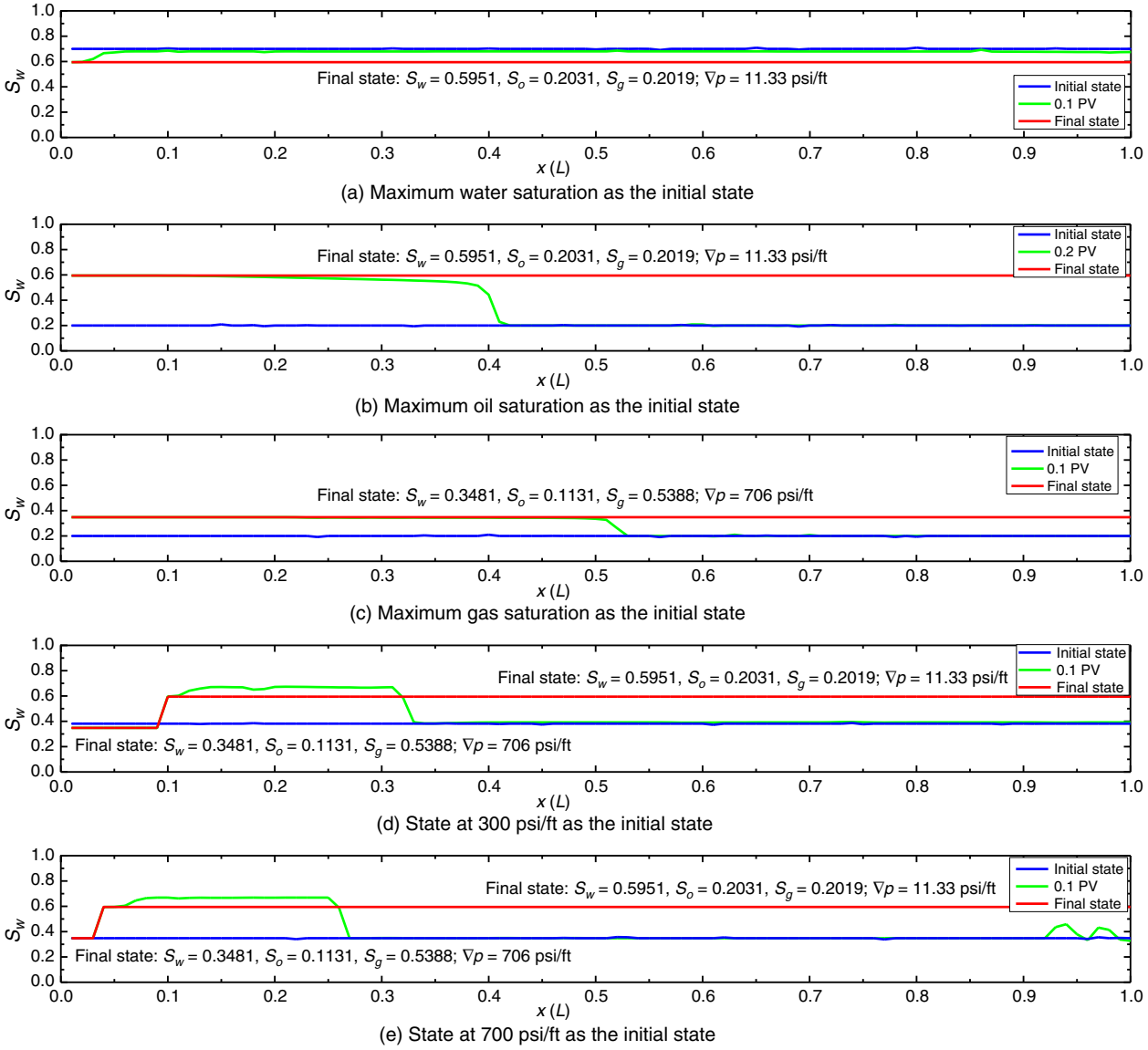

Fig. 17—Final states achieved corresponding to different initial conditions during stability analysis of multiple steady states in Fig. 16, using the 1D simulator excluding capillary diffusion. (a) Maximum water saturation as the initial state; (b) maximum oil saturation as the initial state; (c) maximum gas saturation as the initial state; (d) state at 300 psi/ft as the initial state; (e) state at 700 psi/ft as the initial state.

The initial state plays an important role in determining which state one achieves for given injection conditions. If oil kills foam, as in the dry-out model, it is reasonable that two final states could exist, one with strong foam and one with weak foam or no foam; it is not just an artifact of this model. If the initial oil saturation is high, then oil might kill the foam; at the low-pressure gradient without foam, the small injected oil superficial velocity is sufficient to keep oil saturation constant. On the other hand, with little oil initially in the core, strong foam might carry the injected oil directly out of the core without allowing oil saturation to rise. Thus, in an experimental study of steady-state behavior such as that modeled here, one must be careful of the initial state of the core because hysteresis could play a major part in the behavior observed.

Thus, for this example, there exist three steady states corresponding to one injection condition: one at approximately 706 psi/ft, one at 300 psi/ft, and one at 11.33 psi/ft in this case. The previous analysis missed another intersection of contours at the same superficial velocities.

Third* ∇p *Contour. The simulation results indicate that there must be a contour missing in Fig. 13. A clue comes from extending the range of water and gas superficial velocities in Fig. 13, as illustrated in **Fig. 19.** Although such extreme values of U_w and U_g are not feasible physically, this plot shows the complete pressure-gradient contour predicted by the dry-out model.

Each pressure-gradient contour in Fig. 19 shifts from vertical in the high-quality regime to horizontal in the low-quality regime (extreme lower left on this plot), and then back to the high-quality regime with increasing water superficial velocity. Along this second ascent, foam collapses completely; the remainder of the ascent and descent reflects three-phase flow without foam. Eventually, with increasing water superficial velocity, gas saturation drops to its immobile saturation and the superficial velocity of gas reaches zero.

Fig. 20 shows the complete pressure-gradient contour for 11.45 psi/ft. It shows the same features as in Fig. 19, but at lower superficial velocities. **Fig. 21,** plotted on the scale of Fig. 13, shows this contour and its intersection with the 300- and 700-psi/ft contours.

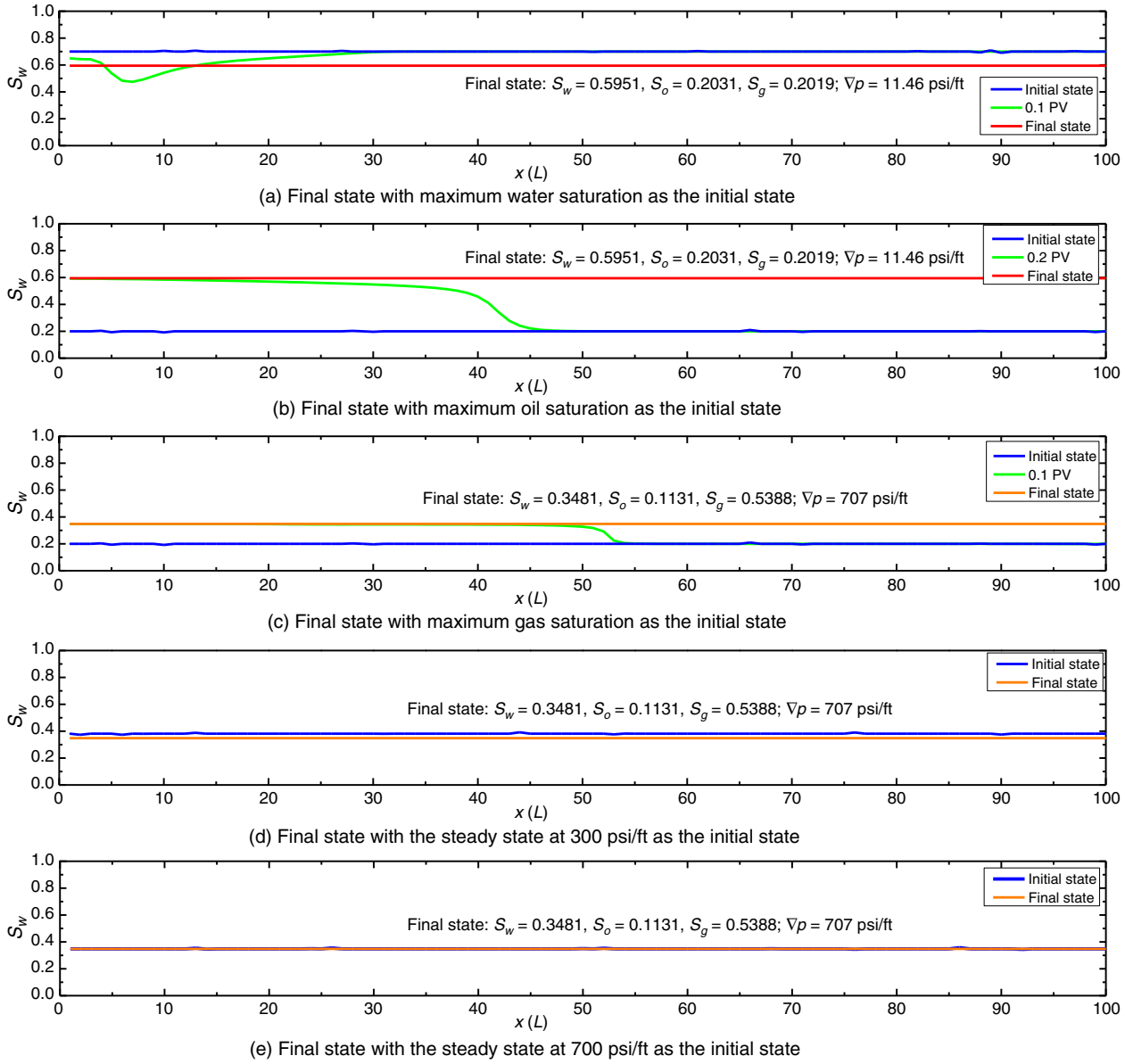

Fig. 18—Final states achieved corresponding to different initial conditions during stability analysis of multiple steady states in Fig. 13, using the 1D simulator with capillary diffusion. (a) Final state with maximum water saturation as the initial state; (b) final state with maximum oil saturation as the initial state; (c) final state with maximum gas saturation as the initial state; (d) final state with the steady state at 300 psi/ft as the initial state; (e) final state with the steady state at 700 psi/ft as the initial state.

Scenario No.		Injection Condition (ft/D)			Initial State			Final State			
		U_w	U_o	U_g	S_w	S_o	S_g	S_w	S_o	S_g	∇p (psi/ft)
1	$S_{w,max}$				0.7	0.1	0.2	0.59510	0.20310	0.20190	11.40
2	$S_{o,max}$				0.2	0.6	0.2	0.59510	0.20310	0.20190	11.40
3	$S_{g,max}$	10.42960	0.40572	2.47777	0.2	0.1	0.7	0.35393	0.11424	0.53184	600.00
4	300 psi/ft				0.38156	0.12014	0.49831	0.35393	0.11424	0.53184	600.00
5	600 psi/ft				0.35393	0.11424	0.53183	0.35390	0.11422	0.53184	600.00

Table 2—Results of numerical stability analysis to a different set of multiple steady states at the intersection of 300- and 600-psi/ft contours from Fig. 13 (with diffusion).

Multiple Steady States as Folds in a Surface. Because we exclude the factor for non-Newtonian effects in the STARS model, all the contours in any plot shown here scale linearly with total superficial velocity. Each point on one contour corresponds to a point on another contour, with the same saturations, at a multiple of the superficial velocities of the first point. Therefore, apparent viscosity is independent of total superficial velocity. For a given model and set of parameters, one can plot μ_{app} (Eq. 1) as a function of the three fractional flows. Because the fractional flows must sum to unity, it is convenient to plot this as a surface over a triangular diagram of fractional flows. An experiment at fixed U_o/U_w corresponds to a trace along this diagram at the same ratio of f_o/f_w, from the corner at $f_g = 1$ to the opposite side of the triangle. All the contours in a plot such as Fig. 11 correspond to one such trace.

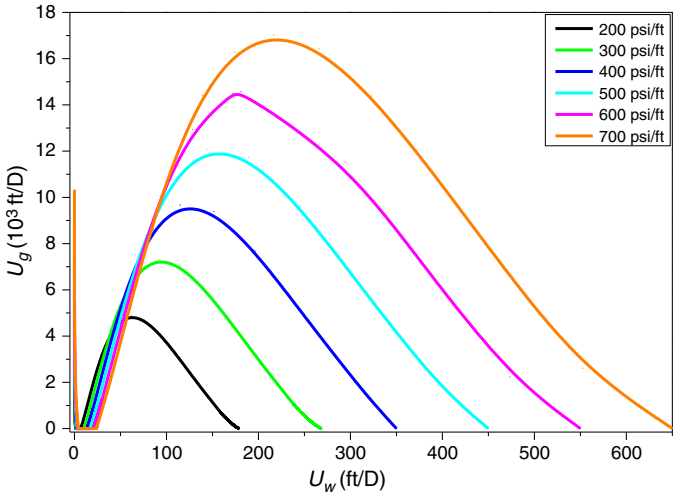

Fig. 19—Extended plot with same parameter values as Fig. 13.

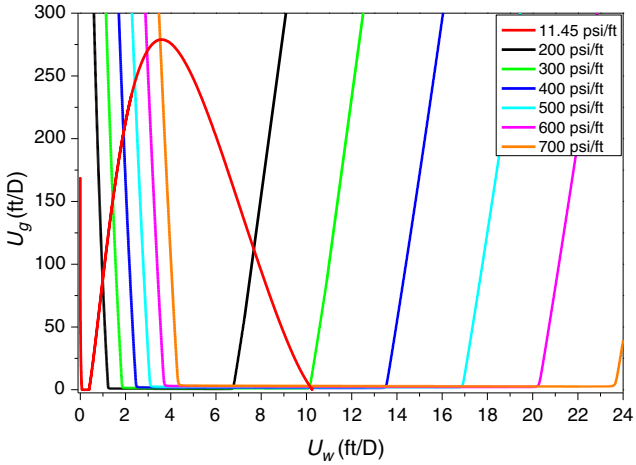

Fig. 20—Replot of Fig. 13, with the missing contour predicted by dry-out model.

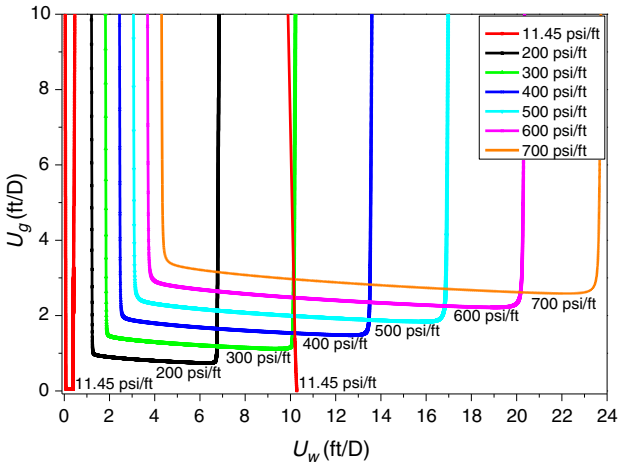

Fig. 21—Replot of Fig. 20, focusing on lower range in gas superficial velocity.

For one set of wet-foam parameters, **Fig. 22** illustrates this surface using its traces at fixed f_o/f_w, equivalent to fixed U_o/U_w. The black curve, above the back edge of the triangle at $f_o = 0$, shows the two flow regimes without oil. The high-quality regime is the right side of this curve, at high gas fractional flow. As U_o/U_w increases, a fold appears, starting from the bottom-right edge of the surface. The bottom, nearly flat, surface corresponds to complete foam collapse. As U_o/U_w increases further, the lobe representing foam shrinks until it disappears; at larger values of U_o/U_w, there is only one steady state, that of fully collapsed foam. **Fig. 23** shows similar behavior for one set of parameters for the dry-foam model.

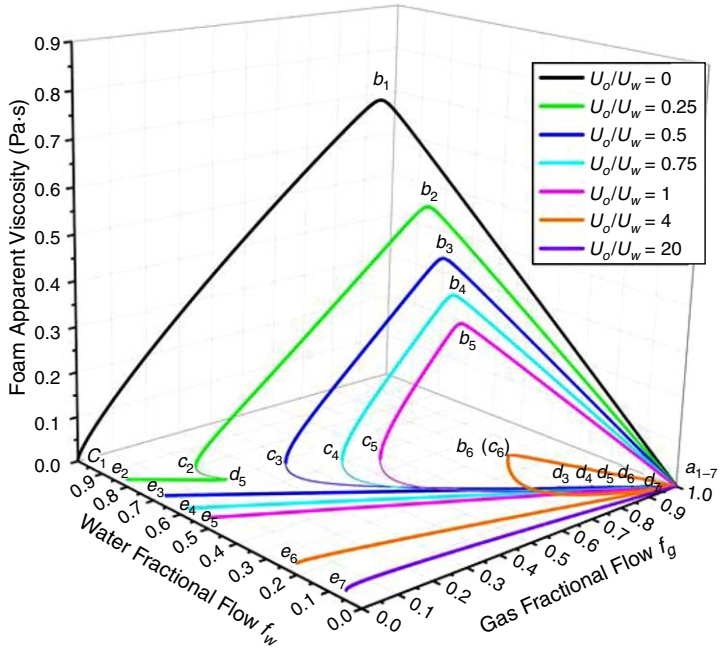

Fig. 22—Foam apparent viscosity as a function of f_w, f_g, and f_o predicted by the wet-foam model with various oil/water-superficial-velocity ratios (*fmoil* = 0.3, *floil* = 0.1, *epoil* = 4). Traces with multiple steady states follow a sequence a_i, b_i, c_i, d_i, e_i; for $f_o = 0$: a_1, b_1, c_1; for $U_o/U_w = 20$: a_i, e_i.

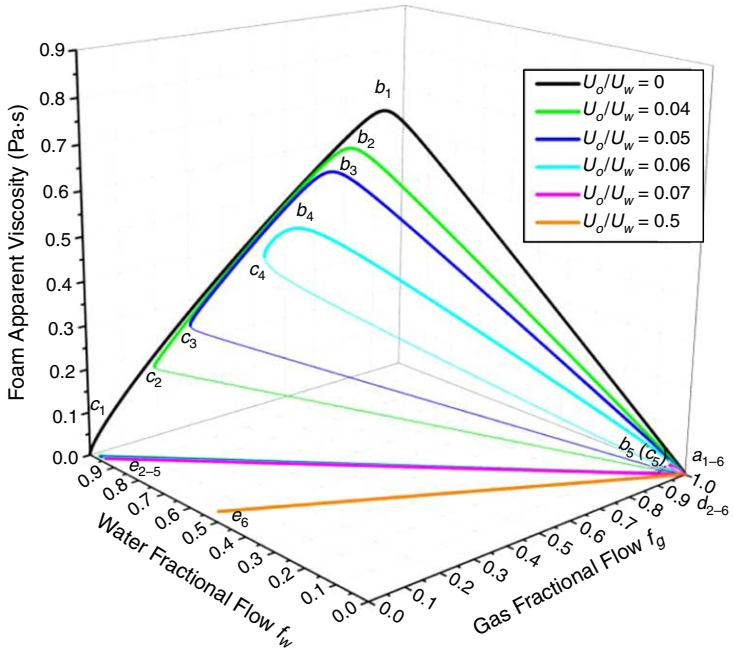

Fig. 23—Foam apparent viscosity as a function of f_w, f_g, and f_o predicted by the dry-out model with various oil/water-superficial-velocity ratios (*sfoil* = 0.144, *sloil* = 0.1, *efoil* = 3). Traces with multiple steady states follow a sequence a_i, b_i, c_i, d_i, e_i; for $f_o = 0$: a_1, b_1, c_1; for $U_o/U_w = 0.5$: a_i, e_i.

Further analysis shows that water saturation increases, following each trace in Fig. 22 starting from the bottom-right edge of the surface (*a*, *b*, *c*, *d*, and *e*), as illustrated in **Fig. 24.** As discussed in the section on multiple steady states, with fixed U_o/U_w, the increase in S_w also means an increase in S_o, suggesting weaker foam along the trace until complete foam collapse, which leads to multiple steady states. The dry-out model predicts similar behavior for foam apparent viscosity plotted on a ternary diagram representing fractional flows, but the occurrence of multiple steady states in Fig. 23 is caused by the value of water saturation relative to limiting water saturation because the latter is modified by oil saturation. The identification of such multiple steady states is of interest in both theoretical study and practical applications. To verify the existence of the multiple steady states and test their stability, one can perform an experiment holding the same injection condition (coinjection of surfactant solution and gas) into a core initially at different conditions (e.g., a core initially saturated with oil or surfactant solution), where multiple steady states are predicted by the foam models under relevant experiment conditions. Given the stability of the multiple steady states, it is speculated that one might end up with the strong and greatly weakened foam states, whereas the middle state is unstable and therefore not observed.

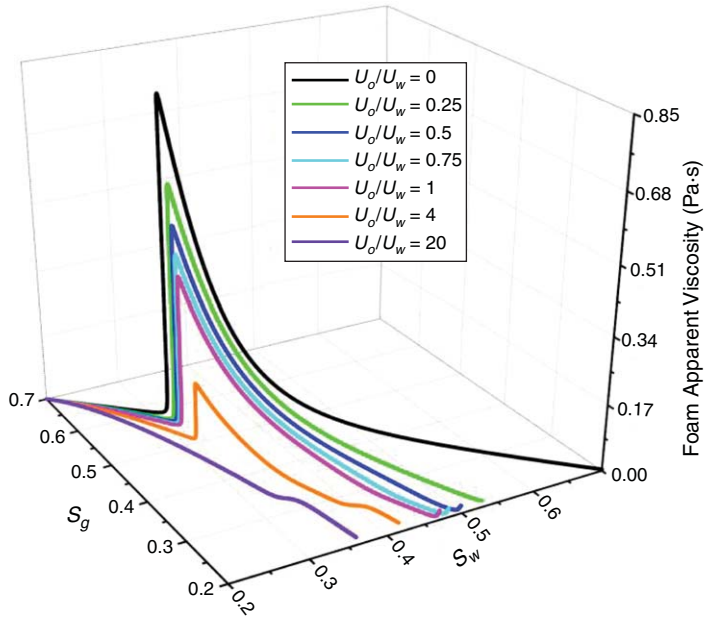

Fig. 24—Foam apparent viscosity as a function of S_w, S_g, and S_o predicted by the wet-foam model for various oil/water-superficial-velocity ratios. All the parameters used are the same as in Fig. 22. Each trace, starting from the bottom-left edge of the surface, corresponds to the path of *a, b, c, d, e* of the corresponding trace in Fig. 22.

This behavior is reminiscent of catastrophe theory (Zeeman 1977), with three steady states represented by a fold in the surface representing the behavior of the system, and the middle state being unstable. The theory states that all equilibrium points of a dependent variable as a function of two independent variables can form a smooth surface, like an "S" shape (Arnold et al. 1999; Wiggins 2013). It suggests that in the folded region between the two edges of the folding surface, there exist three equilibrium points fitting a same set of the two independent variables, which are referred to as multiple steady states in our study. A special feature is that because of the instability of the middle state, only the upper and lower states can be observed depending on the path of independent variables. In consequence, there could be an abrupt change in behavior with a small variation in independent variables. This behavior is similar to the three steady states observed in studies of foam generation without oil (Gauglitz et al. 2002; Kam and Rossen 2003; Lotfollahi et al. 2016b). In that case, in both modeling and experiments, three steady states were observed, with the middle state being unstable.

Discussion and Remarks

This study reveals the way in which current IT foam models represent the effect of oil on steady-state foam-flow dynamics in porous media. In numerical simulation, it is a necessary first step to understand the interaction dynamics of foam with oil as represented in the current models. Results obtained in this study can provide guidance on fitting parameter values. This study does not tell us which model is valid. If a model is valid, it tells how to adjust it to fit data, or helps guide this process, once one has experimental data on the effect of oil on foam. In an experimental study, knowing the effects of model parameters examined on the two foam regimes can assist in interpreting the experimental data. A companion study (Tang et al. 2017) has gathered experimental evidence for the effect of oil on the two foam regimes. Most of the analyses here are consistent with their experimental observations.

Specifically, this study suggests that the wet-foam and dry-out models capture the effects of oil only on the low- and high-quality regimes, respectively. The data of Tang et al. (2017) give evidence for the actual effect of oil on the two regimes, which can guide modeling and numerical simulation for foam flow with oil. Furthermore, both models predict multiple steady states. In the dry-out model, the multiple steady states arise from the interplay between S_w and S_w^*. In the wet-foam model, they arise from the change in *fmmob* with changes in S_o. Experimental evidence is needed to verify the existence of the multiple steady states for foam flow with oil. The preceding stability analysis suggests that the final state achieved for each set of multiple steady states depends on the initial reservoir condition. If such multiple steady states do exist, the injection strategy and initial reservoir conditions for implementing foam EOR, such as where and when to inject foam and the foam quality to be injected, are key for the effectiveness of foam for gas-mobility control.

Conclusions

The STARS foam model has two algorithms to represent the effect of oil saturation on foam: the wet-foam model and the dry-out model. If the transition between high- and low-quality regimes is abrupt, then the parameters in the wet-foam model alter only the low-quality regime, whereas the dry-out model alters the high-quality regime. This information can guide the fitting of model parameters to experimental data for steady-state foam mobility as a function of superficial velocities of water, gas, and oil.

Plotting the apparent foam mobility as a function of injected-foam quality can be confusing if oil is injected as a fixed fraction of the water-injection rate in the experiment. The plot can give the incorrect impression that the wet-foam-model parameters alter the high-quality regime.

The STARS foam model predicts that multiple steady states are possible for some injection conditions and some sets of model parameters. This is not necessarily an artifact of the model; it is plausible that the final steady state achieved with long-time injections of foam and oil might depend, for instance, on initial oil saturation. Multiple steady states are found for both the wet-foam and dry-out models. In this initial study, we find three steady states for some injection conditions: a strong-foam state, one of collapsed foam, and an intermediate state that is unstable to perturbations. If the apparent viscosity is plotted as a function of fractional flows of water, gas, and oil, these states appear as a fold in that surface. This behavior is reminiscent of catastrophe theory and of multiple steady states previously observed in studies of foam generation without oil.

Because of the possibility of multiple steady states, experimental studies of steady-state foam behavior with oil should check for hysteresis and the effect of initial state on their results.

Further Discovery. During the proof stage of this paper, we became aware of another work that presents a population-balance model designed to represent for the effect of oil on foam stability (Ma et al. 2018). This model includes parameters to adjust behavior in both the low- and high-quality regimes, but exactly how is not described in that work.

Nomenclature

D_w, D_g, D_o = capillary-diffusion coefficient for water, gas, and oil, respectively, dimensionless (Eq. 3)
$efoil$ = oil exponent (dry-out model), dimensionless (Eq. A-10)
$epdry$ = water parameter in foam model (wet-foam model), dimensionless (Eq. A-3)
$epoil$ = oil exponent (wet-foam model), dimensionless (Eq. A-4)
$fmdry$ = limiting water saturation (wet-foam model), dimensionless (Eq. A-3)
$fmmob$ = reference-mobility-reduction factor, dimensionless (Eq. A-2)
$floil$ = lower limiting oil saturation on foam (wet-foam model), dimensionless (Eq. A-4)
$fmoil$ = upper limiting oil saturation on foam (wet-foam model), dimensionless (Eq. A-4)
f_w, f_g, f_o = water, gas, and oil fractional flow, respectively, fraction
f_g^* = transition foam quality from low- to high-quality regime
f_{p0} = fractional flows into first gridblock, fraction
F_1 = effect of surfactant concentration on foam, dimensionless (Eq. A-2)
F_2 = effect of water saturation on foam, dimensionless (Eq. A-3)
F_3 = effect of oil saturation on foam, dimensionless (Eq. A-4)
F_4 = effect of gas superficial velocity on foam, dimensionless (Eq. A-2)
F_5 = effect of shear-thinning rheology on foam, dimensionless (Eq. A-2)
F_6 = effect of critical capillary number on foam, dimensionless (Eq. A-2)
F_7 = effect of water saturation on foam (dry-out model), dimensionless (Eq. A-9)
FM = mobility reduction factor, dimensionless (Eq. A-2)
G_2 = effect of oil saturation on foam (dry-out model), dimensionless (Eq. A-10)
k = permeability, m^2
k_{rg} = foam free-gas relative permeability, dimensionless
k_{rg}^f = effective gas relative permeability with foam, dimensionless
k_{rw}, k_{ro} = water and oil relative permeability, respectively, dimensionless
$k_{rw}^0, k_{rg}^0, k_{ro}^0$ = endpoint relative permeabilities of water, gas, and oil, respectively, dimensionless
n_g = gas exponent for Corey relative permeability, dimensionless
n_o = oil exponent for Corey relative permeability, dimensionless
n_w = water exponent for Corey relative permeability, dimensionless
PV = pore volumes dimensionless
$sfbet$ = water parameter in foam model (dry-out model), dimensionless (Eq. A-9)
$sfdry$ = limiting water saturation (dry-out model), dimensionless (Eq. A-11)
$sfoil$ = upper-limiting oil saturation on foam (dry-out model), dimensionless (Eq. A-10)
$sloil$ = lower-limiting oil saturation on foam (dry-out model), dimensionless (Eq. A-10)
$S_{g,\max}$ = maximum gas saturation at residual of the other two phases, fraction
S_{gr} = residual gas saturation, fraction
$S_{o,\max}$ = maximum oil saturation at residual of the other two phases, fraction
S_{or} = residual oil saturation, fraction
S_w, S_o, S_g = water, oil, and gas saturation, respectively, fraction
$S_{w,\max}$ = maximum water saturation at residual of the other two phases, fraction
S_{wc} = connate-water saturation, fraction
U_t = total superficial velocity, m/s
U_w, U_g, U_o = water, gas, and oil superficial velocity, respectively, m/s
∇p = pressure gradient, Pa/m
Δt = timestep of each iteration, seconds
Δx = gridblock size, m
μ_{app} = foam apparent viscosity, Pa·s
μ_w, μ_g, μ_o = water, gas, and oil viscosity, respectively, Pa·s
ϕ = porosity, fraction

Superscripts

f = foam
o = endpoint relative permeability

Subscripts

i = gridblock of length Δx
p = water, gas, or oil phase

Acknowledgments

This study was funded in part by the Joint Industry Project on Foam for EOR at Delft University of Technology, and also by the Chinese Scholarship Council. We thank Dan Marchesin of IMPA, Brazil, for helpful comments on this work.

References

Al Sumaiti, A., Shaik, A. R., Mathew, E. S. et al. 2017. Tuning Foam Parameters for Mobility Control Using CO_2 Foam: Field Application To Maximize Oil Recovery From a High Temperature High Salinity Layered Carbonate Reservoir. *Energy Fuels* **31** (5): 4637–4654. https://doi.org/10.1021/acs.energyfuels.6b02595.

Alvarez, J. M., Rivas, H. J., and Rossen, W. R. 2001. A Unified Model for Steady-State Foam Behavior at High and Low Foam Qualities. *SPE J.* **6** (3): 325–333. SPE-74141-PA. https://doi.org/10.2118/74141-PA.

Arnold, V. I., Kazarinoff, N., Afrajmovich, V. S. et al. 1999. *Dynamical Systems V: Bifurcation Theory and Catastrophe Theory*. Berlin: Springer.

Basheva, E. S., Ganchev, D., Denkov, N. D. et al. 2000. Role of Betaine as Foam Booster in the Presence of Silicone Oil Drops. *Langmuir* **16** (3): 1000–1013. https://doi.org/10.1021/la990777+.

Bergeron, V., Fagan, M. E., and Radke, C. J. 1993. Generalized Entering Coefficients: A Criterion for Foam Stability Against Oil in Porous Media. *Langmuir* **9** (7): 1704–1713. https://doi.org/10.1021/la00031a017.

Boeije, C. S. and Rossen, W. 2015. Fitting Foam-Simulation-Model Parameters To Data: I. Coinjection of Gas and Liquid. *SPE Res Eval & Eng* **18** (2): 264–272. SPE-174544-PA. https://doi.org/10.2118/174544-PA.

Cheng, L., Reme, A. B., Shan, D. et al. 2000. Simulating Foam Processes at High and Low Foam Qualities. Presented at the SPE/DOE Improved Oil Recovery Symposium, Tulsa, 3–5 April. SPE-59287-MS. https://doi.org/10.2118/59287-MS

Computer Modelling Group (CMG). 2015. *STARS User's Guide, Version 2015*. Calgary: CMG.

Dalland, M., Hanssen, J. E., and Kristiansen, T. S. 1994. Oil Interaction With Foams Under Static and Flowing Conditions in Porous Media. *Colloid. Surface. A* **82** (2): 129–140. https://doi.org/10.1016/0927-7757(93)02628-R.

de Araujo Cavalcante Filho, J. S., Delshad, M., and Sepehrnoori, K. 2018. Estimation of Foam-Flow Parameters for Local Equilibrium Methods by Use of Steady-State Flow Experiments and Optimization Algorithms. *SPE Res Eval & Eng* **21** (1): 160–173. SPE-179597-PA. https://doi.org/10.2118/179597-PA.

Falls, A. H., Hirasaki, G. J., Patzek, T. W. et al. 1988. Development of a Mechanistic Foam Simulator: The Population Balance and Generation by Snap-Off. *SPE Res Eng* **3** (3): 884–892. SPE-14961-PA. https://doi.org/10.2118/14961-PA.

Farajzadeh, R., Andrianov, A., Krastev, R. et al. 2012. Foam–Oil Interaction in Porous Media: Implications for Foam Assisted Enhanced Oil Recovery. *Adv. Colloid Interf. Sci.* **183–184** (15 November): 1–13. https://doi.org/10.1016/j.cis.2012.07.002.

Farajzadeh, R., Lotfollahi, M., Eftekhari, A. A. et al. 2015. Effect of Permeability on Implicit-Texture Foam Model Parameters and the Limiting Capillary Pressure. *Energy Fuels* **29** (5): 3011–3018. https://doi.org/10.1021/acs.energyfuels.5b00248.

Frye, G. C. and Berg, J. C. 1989. Antifoam Action by Solid Particles. *J. Colloid Interf. Sci.* **127** (1): 222–238. https://doi.org/10.1016/0021-9797(89)90023-4.

Garrett, P. R. 1979. The Effect of Polytetrafluoroethylene Particles on the Foamability of Aqueous Surfactant Solutions. *J. Colloid Interf. Sci.* **69** (1): 107–121. https://doi.org/10.1016/0021-9797(79)90085-7.

Gauglitz, A. P., Friedmann, F., Kam, S. I. et al. 2002. Foam Generation in Homogeneous Porous Media. *Chem. Eng. Sci.* **57** (19): 4037–4052. https://doi.org/10.1016/S0009-2509(02)00340-8.

Hahn, P.-S., Ramamohan, T. R., and Slattery, J. C. 1985. Mobility Control in the Displacement of Residual Oil by an Unstable Foam. *AIChE J.* **31** (6): 1029–1035. https://doi.org/10.1002/aic.690310620.

Harkins, W. D. and Feldman, A. 1922. Films: The Spreading of Liquids and the Spreading Coefficient. *J. Am. Chem. Soc.* **44** (12): 2665–2685. https://doi.org/10.1021/ja01433a001.

Hirasaki, G. J. and Lawson, J. B. 1985. Mechanisms of Foam Flow in Porous Media: Apparent Viscosity in Smooth Capillaries. *SPE J.* **25** (2): 176–190. SPE-12129-PA. https://doi.org/10.2118/12129-PA.

Kam, S. I. and Rossen, W. R. 2003. A Model for Foam Generation in Homogeneous Media. *SPE J.* **8** (4): 417–425. SPE-87334-PA. https://doi.org/10.2118/87334-PA.

Kapetas, L., Vincent Bonnieu, S., Farajzadeh, R. et al. 2017. Effect of Permeability on Foam-Model Parameters: An Integrated Approach From Core-Flood Experiments Through to Foam Diversion Calculations. *Colloid. Surface. A* **530** (5 October): 172–180. https://doi.org/10.1016/j.colsurfa.2017.06.060.

Khatib, Z. I., Hirasaki, G. J., and Falls, A. H. 1988. Effects of Capillary Pressure on Coalescence and Phase Mobilities in Foams Flowing Through Porous Media. *SPE Res Eng* **3** (3): 919–926. SPE-15442-PA. https://doi.org/10.2118/15442-PA.

Kim, J., Dong, Y., and Rossen, W. R. 2005. Steady-State Flow Behavior of CO_2 Foam. *SPE J.* **10** (4): 405–415. SPE-89351-PA. https://doi.org/10.2118/89351-PA.

Kruglyakov, P. M. and Vilkova, N. G. 1999. The Relation Between Stability of Asymmetric Films of the Liquid/Liquid/Gas Type, Spreading Coefficient and Surface Pressure. *Colloid. Surface. A.* **156** (1): 475–487. https://doi.org/10.1016/S0927-7757(99)00105-3.

Lake, L. W., Johns, R. T., Rossen, W. R. et al. 2014. *Fundamentals of Enhanced Oil Recovery*. Richardson, Texas: Society of Petroleum Engineers.

Lotfollahi, M., Farajzadeh, R., Delshad, M. et al. 2016a. Comparison of Implicit-Texture and Population-Balance Foam Models. Presented at the SPE EOR Conference at Oil and Gas West Asia, Muscat, Oman, 21–23 March. SPE-179808-MS. https://doi.org/10.2118/179808-MS.

Lotfollahi, M., Kim, I., Beygi, M. R. et al. 2016b. Experimental Studies and Modeling of Foam Hysteresis in Porous Media. Presented at SPE Improved Oil Recovery Conference, Tulsa, 11–13 April. SPE-179664-MS. https://doi.org/10.2118/179664-MS.

Ma, K., Lopez-Salinas, J. L., Puerto, M. C. et al. 2013. Estimation of Parameters for the Simulation of Foam Flow Through Porous Media. Part 1: The Dry-Out Effect. *Energy Fuels* **27** (5): 2363–2375. https://doi.org/10.1021/ef302036s.

Ma, K., Mateen, K., Ren, G. et al. 2018. Mechanistic Modeling of Foam Flow Through Porous Media in the Presence of Oil: Review of Foam-Oil Interactions and an Improved Bubble Population-Balance Model. Presented at the SPE Annual Technical Conference and Exhibition, Dallas, 24–26 September. SPE-191564-MS. https://doi.org/10.2118/191564-MS.

Ma, K., Ren, G., Mateen, K. et al. 2015. Modeling Techniques for Foam Flow in Porous Media. *SPE J.* **20** (3): 453–470. SPE-169104-PA. https://doi.org/10.2118/169104-PA.

Myers, T. J. and Radke, C. J. 2000. Transient Foam Displacement in the Presence of Residual Oil: Experiment and Simulation Using a Population-Balance Model. *Ind. Eng. Chem. Res.* **39** (8): 2725–2741. https://doi.org/10.1021/ie990909u.

Osterloh, W. T. and Jante, M. J. Jr. 1992. Effects of Gas and Liquid Velocity on Steady-State Foam Flow at High Temperature. Presented at the SPE/DOE Enhanced Oil Recovery Symposium, Tulsa, 22–24 April. SPE-24179-MS. https://doi.org/10.2118/24179-MS.

Rong, J. G. 2002. *Experimental Evaluation of Foam in Environmental Remediation*. PhD dissertation, University of Texas at Austin, Austin, Texas (May 2002).

Rossen, W. R. 1996. Foams in Enhanced Oil Recovery. In *Foams: Theory, Measurements, and Applications*, ed. R. K. Prud'homme and S. Khan, 413–464. New York City: Marcel Dekker.

Rossen, W. R. and Wang, M.-W. 1997. Modeling Foams for Acid Diversion. Presented at SPE European Formation Damage Conference, The Hague, 2–3 June. SPE-38200-MS. https://doi.org/10.2118/38200-MS.

Schramm, L. L. ed. 1994. *Foams: Fundamentals and Applications in the Petroleum Industry*. Washington, DC: American Chemical Society.

Shen, C., Nguyen, Q. P., Huh, C. et al. 2006. Does Polymer Stabilize Foam in Porous Media? Presented at the SPE/DOE Symposium on Improved Oil Recovery, Tulsa, 22–26 April. SPE-99796-MS. https://doi.org/10.2118/99796-MS.

Simjoo, M. and Zitha, P. L. J. 2013. Effects of Oil on Foam Generation and Propagation in Porous Media. Presented at the SPE Enhanced Oil Recovery Conference, Kuala Lumpur, 2–4 July. SPE-165271-MS. https://doi.org/10.2118/165271-MS.

Tang, J., Vincent-Bonnieu, S., and Rossen, W. R. 2017. The Effect of Oil on Steady-State Foam Flow Regimes in Porous Media. Presented at the IOR 2017–19th European Symposium on Improved Oil Recovery, Stavanger, Norway, 24–27 April.

Wiggins, S. 2013. *Global Bifurcations and Chaos: Analytical Methods*. New York City: Springer.

Xu, Q. and Rossen, W. R. 2003. Effective Viscosity of Foam in Periodically Constricted Tubes. *Colloid. Surface. A* **216** (1): 175–194. https://doi.org/10.1016/S0927-7757(02)00547-2.

Zeeman, E. C. 1977. *Catastrophe Theory: Selected Papers, 1972–1977*. Boston, Massachusetts: Addison-Wesley.

Zeng, Y., Muthuswamy, A., Ma, K. et al. 2016. Insights on Foam Transport From a Texture-Implicit Local-Equilibrium Model With an Improved Parameter Estimation Algorithm. *Ind. Eng. Chem. Res.* **55** (28): 7819–7829. https://doi.org/10.1021/acs.iecr.6b01424.

Appendix A—Foam Models

The widely used STARS (CMG 2015) foam model includes two algorithms to represent the influence of oil on foam: the wet-foam model and the dry-out model. More details pertaining to these two models are provided here.

Wet-Foam Model. In this model, it is assumed that the presence of foam affects the relative permeability of gas, but not that for water or for oil. In the model, foam modifies the foam-free relative permeability of gas k^0_{rg} by multiplying by FM,

$$k^f_{rg} = k^0_{rg} \times FM, \quad \text{(A-1)}$$

where k^f_{rg} is the effective gas relative permeability with foam. A smaller value of FM indicates stronger foam, whereas FM equal to unity means no foam exists.

The FM is given by Eq. A-2; it depends on a series of functions (F_1, F_2, F_3, and so forth), reflecting the dependence of foam on surfactant concentration, water saturation, oil saturation, capillary number, oil composition, and salinity, respectively (Cheng et al. 2000; CMG 2015):

$$FM = \frac{1}{1 + fmmob \times F_1 \times F_2 \times F_3 \times F_4 \times F_5 \times F_6 \ldots}, \quad \text{(A-2)}$$

where the parameter *fmmob* is the reference-mobility-reduction factor in a situation where all conditions yield maximum foam strength. The factors F_i are given different subscripts in different references.

In this paper, we consider only the water-saturation-dependent function F_2 and the oil-dependent function F_3 given by

$$F_2 = 0.5 + \frac{\arctan[epdry(S_w - fmdry)]}{\pi}, \quad \text{(A-3)}$$

$$F_3 = \begin{cases} 1, & S_o \le floil \\ \left(\dfrac{fmoil - S_o}{fmoil - floil}\right)^{epoil}, & floil < S_o < fmoil \\ 0, & fmoil \le S_o \le 1 - S_{wc} - S_{gr}. \end{cases} \quad \text{(A-4)}$$

An abrupt transition between low- and high-quality foam-flow regimes corresponds to a large value of *epdry*. **Table A-1** gives the definitions of the parameters in Eqs. A-3 and A-4. We use Corey relations for the foam-free relative permeabilities for water, oil, and gas,

$$k_{rw} = k^o_{rw}\left(\frac{S_w - S_{wc}}{1 - S_{wc} - S_{or} - S_{gr}}\right)^{n_w}, \quad \text{(A-5)}$$

$$k_{ro} = k^o_{ro}\left(\frac{S_o - S_{or}}{1 - S_{wc} - S_{or} - S_{gr}}\right)^{n_o}, \quad \text{(A-6)}$$

$$k_{rg} = k^o_{rg}\left(\frac{S_g - S_{gr}}{1 - S_{wc} - S_{or} - S_{gr}}\right)^{n_g}, \quad \text{(A-7)}$$

where k^0_{rw}, k^0_{ro}, and k^0_{rg} are each the endpoint relative permeability, and n_w, n_o, and n_g are the Corey exponents for the given phase. The larger the Corey exponent of a given phase, the more wetting it is to rock.

Parameters	Definition
fmmob	Reference-mobility-reduction factor corresponding to maximum foam strength.
fmdry, *sfdry*	Limiting water saturation, around which foam collapses, for wet-foam and dry-out models, respectively. The value of *sfdry* is not a fixed constant, but is instead a function of oil saturation.
epdry, *sfbet*	Parameter determining how abruptly gas mobility changes for water saturation near *fmdry* or *sfdry* for wet-foam and dry-out models, respectively.
fmoil, *sfoil*	Upper-limiting oil saturation, greater than which foam collapses completely for wet-foam and dry-out models, respectively.
floil, *sloil*	Lower-limiting oil saturation,less than which oil has no detrimental effect on foam for wet-foam and dry-out models, respectively.
epoil, *efoil*	Exponent for oil effect for wet-foam and dry-out models, respectively.

Table A-1—An overview of foam-simulation-parameter definitions.

Table A-2 summarizes all the model-parameter values examined except for the oil-related parameters specified in each figure in the text. The same parameter values are used throughout this paper unless otherwise specified.

Foam-Model Parameters			Corey-Relation Parameters								
fmmob	*fmdry/sfdry*	*epdry/sfbet*	k_{rw}^0	k_{ro}^0	k_{rg}^0	n_w	n_o	n_g	S_{wc}	S_{or}	S_{gr}
54,000	0.316	6,000	0.20	0.50	0.94	4.2	2.0	1.3	0.2	0.1	0.2
			Rock and Fluid Properties								
D_w	D_o	D_g	*k* (darcies)	ϕ	μ_w (Pa·s)		μ_o (Pa·s)		μ_g (Pa·s)		
3	3	3	1.3	0.3	7.00×10^{-4}		5.00×10^{-3}		2.07×10^{-5}		

Table A-2—An overview of STARS foam model parameters used.

Dry-Out Model. The form of the dry-out model is similar to that of the wet-foam model, except that the limiting water saturation is no longer a constant. Here, we consider the dry-out and wet-foam models for oil and foam separately, although they can be used together in the STARS model. Therefore, for the dry-out model, FM here is given by

$$FM = \frac{1}{1 + fmmob \times F_7}, \quad \text{(A-8)}$$

where F_7 is a water-saturation-dependent function,

$$F_7 = 0.5 + \frac{\arctan[sfbet(S_w - sfdry)]}{\pi}. \quad \text{(A-9)}$$

The parameters *sfbet* and *sfdry* play the roles of *epdry* and *fmdry* in the wet-foam model, respectively, but limiting water saturation *sfdry* in the dry-out model is scaled by a series of functions accounting for the effects of surfactant concentration, oil saturation, salinity, and capillary number, represented with symbols G_1, G_2, G_3, and G_4, respectively. Here, we consider only the effect of oil saturation, reflected in G_2, and given by

$$G_2 = \begin{cases} 0, & S_o \le sloil \\ \left(\dfrac{S_o - sloil}{sfoil - sloil}\right)^{efoil}, & sloil < S_o < sfoil \\ 1, & sfoil \le S_o \le 1 - S_{wc} - S_{gr}, \end{cases} \quad \text{(A-10)}$$

where the upper-limiting oil saturation *sfoil* and lower-limiting oil saturation *sloil* play roles similar to *fmoil* and *floil,* respectively, in the wet-foam model. The original, oil-free value of the limiting water saturation *sfdry* is then rescaled by

$$[(1 - sfdry) \times G_2 + sfdry] \rightarrow sfdry. \quad \text{(A-11)}$$

If S_o is less than *sloil,* $G_2 = 0$ and oil has no detrimental effect on foam. The limiting water saturation, *sfdry,* is then equal to its oil-free value. If S_o is larger than *sfoil,* $G_2 = 1$ and $sfdry = 1$. If the transition between regimes is abrupt (*sfbet* is sufficiently large), foam collapses completely at all water saturations. For S_o between these two values, G_2 lies in between zero and unity, and *sfdry* takes a value between its oil-free value and unity.

Substituting the limiting water saturation as modified by Eqs. A-10 and A-11 into Eq. A-9 allows one to obtain FM accounting for the effects of oil and water saturations. The Corey relations for foam-free relative permeabilities and the same model parameters as in Table A-2 are applied in the dry-out model, also with oil-related parameters specified in each figure in the text.

Jinyu Tang has been a PhD-degree researcher in the Department of Geoscience and Engineering at Delft University of Technology since 2014. His research interests include foams for EOR, multiobjective computed-tomography corefloods, IT foam modeling, and fractional-flow analysis of complex multiphase flow through porous media. Tang holds a master's degree in petroleum engineering from China University of Petroleum. He has been an SPE member since 2014.

Mohammed N. Ansari holds a master's degree in petroleum engineering and geosciences from Delft University of Technology. His work there focused on local-equilibrium modeling of foam dynamics. He has been an SPE member since 2014.

William R. Rossen is a professor of reservoir engineering at the Department of Geoscience and Engineering at Delft University of Technology. His current research concerns the use of foams for diverting fluid flow in porous media, modeling complex transport processes in networks, and understanding flow in naturally fractured geological formations. Rossen was named the Best Instructor at Delft University of Technology in 2011. In 2012, he was named an IOR Pioneer at the SPE/DOE Symposium on Improved Oil Recovery in Tulsa. Rossen is an SPE Distinguished Member.